MagDesk: Interactive Tabletop Workspace based on Passive Magnetic Tracking

KUNPENG HUANG, University of Michigan, USA
YASHA IRAVANTCHI, University of Michigan, USA
DONGYAO CHEN, Shanghai Jiao Tong University, China
ALANSON P. SAMPLE, University of Michigan, USA

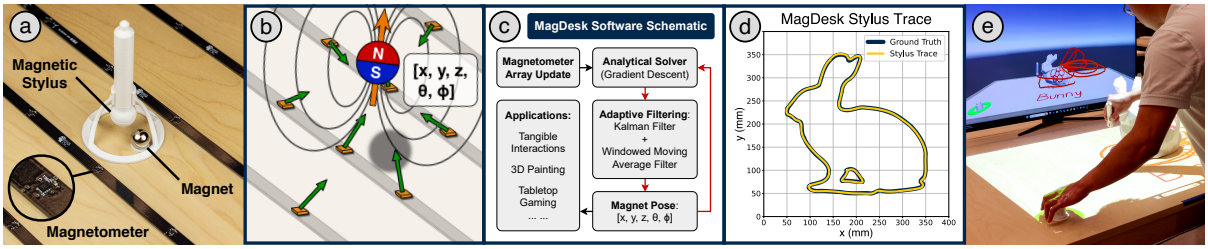

Fig. 1. MagDesk uses an array of 112 low-cost magnetometers to track multiple magnets in 3D with millimeter accuracy across an expansive workspace. Magnets' compact sizes allow them to be embedded in daily objects such as a stylus as trackers (a). MagDesk models each magnet as a magnetic dipole (b) and employs an analytical solver combined with an adaptive filtering pipeline to determine the 5-DoF pose of the magnet and enable diverse interactive applications (c). Using a magnetic stylus, the user is able to recreate digital 2D drawings that closely align with ground truth images (d), as well as sketch arbitrary 3D traces in an augmented-reality environment for artistic expression (e).

Accurate and responsive 3D tracking enables interactive and context-aware workspaces, including mixed reality 3D interfaces and collaborative tangible interactions. However, limitations of current tracking mechanisms – line-of-sight occlusion, drifting errors, small working volumes, or instrumentation that requires maintenance – ultimately restrict their adoption. This paper introduces MagDesk, an interactive tabletop workspace capable of real-time 3D tracking of passive magnets embedded in objects. Using a sensing array of 112 low-cost magnetometers underneath a table, our custom-designed signal processing and localization engine enables simultaneous tracking of multiple magnets in 5 degrees of freedom with millimeter accuracy. MagDesk can continuously and robustly track magnets at a maximum height of *600 mm* over a *1750 mm* (L) × *950 mm* (W) table, while achieving an average positional and orientational error of *2.49 mm* and *0.72°* near the table surface and *14.40 mm* and *2.25°* across the entire sensing range. To demonstrate MagDesk's object-tracking capabilities, this work presents a series of magnetic widgets for tangible interactions and explores two applications – a 3D drawing interface and augmented-reality tabletop games. By instrumenting a regular table surface, MagDesk presents a low-cost and accurate approach to 3D tracking passive objects for home and office environments.

Authors' Contact Information: Kunpeng Huang, University of Michigan, Ann Arbor, MI, USA, kunpeng@umich.edu; Yasha Iravantchi, University of Michigan, Ann Arbor, MI, USA, yiravan@umich.edu; Dongyao Chen, Shanghai Jiao Tong University, Shanghai, China, chendy@sjtu.edu.cn; Alanson P. Sample, University of Michigan, Ann Arbor, MI, USA, apsample@umich.edu.

ACM 2474-9567/2024/12-ART170
https://doi.org/10.1145/3699756

CCS Concepts: • **Human-centered computing → Interactive systems and tools**; **Ubiquitous and mobile computing systems and tools**.

Additional Key Words and Phrases: Magnetic Sensing, Object Tracking, Interactive Workspace

ACM Reference Format:
Kunpeng Huang, Yasha Iravantchi, Dongyao Chen, and Alanson P. Sample. 2024. MagDesk: Interactive Tabletop Workspace based on Passive Magnetic Tracking. *Proc. ACM Interact. Mob. Wearable Ubiquitous Technol.* 8, 4, Article 170 (December 2024), 31 pages. https://doi.org/10.1145/3699756

1 Introduction

Interactive tabletop workspaces offer opportunities for improved productivity, multi-user collaboration, and new modalities for gaming and entertainment. The prior works on the office of the future (i.e., Office 2.0) in the early 1990s, implemented with video tracking and overhead projection, aimed to provide natural and expressive interactions and demonstrated new possibilities to bridge the physical and digital worlds [47]. More recent research has focused on 3D-tracked gesture-based interfaces [40, 48], tangible interaction with intuitive and accessible control [43, 51], and context-aware augmented reality environments [6, 8]. The ability to precisely track objects and body movements in real-time expands the interaction space beyond 2D surfaces such as tabletops and screens, enabling a more immersive and engaging user experience. However, one of the key challenges preventing these applications from realizing their full potential is achieving cost-effective, accurate, and robust 3D tracking in a tabletop environment.

Common approaches for sensing an object or body's position in a table-sized workspace include optical tracking and using Inertial Measurement Units (IMUs). Optical tracking implementations include outside-in, where cameras are placed in fixed locations in the environment to track the positions of markers on the object [2]; or inside-out, where the camera or sensor is installed on the tracked device and determines its location relative to external references, such as the Lighthouse system used by the HTC Vive [3]. Both approaches require a direct line-of-sight (LoS) between the tracked device and sensors or markers installed externally, limiting their adoptions in workspace environments. IMUs alleviate the LoS issue as they can be placed directly on the tracked object without reliance on external references [2]. However, they suffer from the drifting problem where the estimated position accumulates errors over time. Furthermore, IMUs are powered devices: battery weight and charging requirements place additional burdens on the user for all-day usage. Therefore, an alternative tracking modality is desired for a workspace environment that is accurate, stable, and requires minimum instrumentation.

This paper presents MagDesk, an interactive tabletop workspace for 3D object tracking utilizing passive magnets and an array of embedded magnetometers. Since common materials with low magnetic permeability (e.g., wood, plastic, aluminum, rubber, human tissue, etc.) do not disturb the magnetic fields [18], magnetic sensing enables tracking resilience to the LoS occlusion. The compact sizes of permanent magnets allow them to be easily integrated into daily objects as trackers without charging, achieving robust tracking with minimum maintenance.

MagDesk's sensing platform comprises a 112-magnetometer array placed underneath a regular table, enabling a large sensing volume of *1750 mm* (L) × *950 mm* (W) × *600 mm* (H). Its software adopts the Levenberg–Marquardt (LM) algorithm with an optimized filtering pipeline to simultaneously track multiple spherical magnets in 5 DoF (3D spatial + 2D angular) at 32 Hz with millimeter accuracy. The pipeline combines a Kalman filter and a moving average filter with parameters automatically adapted to magnet sizes, tracking heights, and estimated speeds.

To evaluate the tracking performance of MagDesk, the coordinates of tracked magnets are compared to the ground truth measured by the HTC Vive Trackers [3]. With a 3/4 in.-diameter magnet, MagDesk can achieve positional and orientational accuracy of ***2.49 mm*** and ***0.72***° near the table surface (within *50 mm*), respectively. The maximum trackable height reaches *600 mm* while sustaining stable and continuous tracking, with an average positional and orientational error of ***14.40 mm*** and ***2.25***° across the entire sensing range. Note that the *600 mm*

height doubles the tracking range achieved in prior works that explore passive magnetic tracking and provide full 3D coordinates [10, 44]. In addition, MagDesk's algorithm allows two magnets to be tracked at once, even if they are close to each other. Within *50 mm* above the table surface, the average tracking accuracies are *11.18 mm* and *2.54°* when two 5/8 in.-diameter magnets are as close as *30 mm* apart. Further, MagDesk could track three or more magnets simultaneously and independently by segmenting the magnetometer array into regions. To investigate the possibilities of integrating permanent magnets into daily objects for 3D tracking, this paper also includes a comprehensive evaluation of the tracking heights and accuracies of different magnet sizes (1 in., 3/4 in., 5/8 in., and 1/2 in.-diameter).

As an interactive tabletop workspace, MagDesk's extensive sensing range and robust tracking performance enable a broad range of applications. This paper introduces and evaluates eight magnet-embedded tangible primitives that serve as trackable digital input devices. In addition, two representative usage scenarios are presented and evaluated, including a 3D drawing interface with a magnetic stylus and tangible interaction demonstrated through augmented-reality games controlled by magnetic widgets. These applications demonstrate MagDesk's potential to be integrated into home or office environments.
This paper makes the following contributions:

(1) A real-time magnetic tracking algorithm with adaptive filtering, enabling accurate and robust tracking;
(2) A passive multi-magnet tracking approach with *600 mm* sensing range;
(3) A series of eight magnetic primitives for intuitive tangible interactions;
(4) A demonstration of MagDesk's real-world applications with two example usage scenarios and user evaluations.

2 Related Work

This section details work related to MagDesk, first by providing an overview of the sensing approaches for tracking objects in general and then narrowing the focus towards systems that support making surfaces interactive. Finally, we contextualize MagDesk within other magnetic sensing and tracking approaches.

2.1 Object Tracking Systems

Tracking the position of specific objects remains an active research area within ubiquitous computing and human-computer interaction, and the requirements of end-user applications have motivated the creation of many tracking methods. These applications influence the resolution requirements of tracking (e.g., centimeter-level, millimeter-level), the distance capabilities (e.g., desk-scale, room-scale, floor-scale), and other instrumentation or deployment factors (e.g., Line-of-Sight (LoS) requirements, installation of markers). As a result, numerous approaches offer unique advantages and disadvantages for a given usage scenario.

A predominant approach has been optical or computer vision (CV) tracking, which can optionally include optical markers (such as in mo-cap). Within the "tabletop" scale, Dodecapen [49] uses a dodecahedron of mini fiducial tags to localize and extract the orientation of a pen. To achieve markerless 3D tracking, Comport et al. [16] utilize multiple camera views to track an object in real-time and, more recently, state-of-the-art (SoTA) high-precision 3D object tracking approaches presented by Li et al. [28] find millimeter-level tracking accuracy. However, while multiple camera views can relax the LoS requirement (i.e., the system has more opportunities for an unobstructed view), there are many common scenarios where no unobstructed view is available, such as if the object is being held within a closed hand. In addition, installing multiple cameras around the environment incurs additional instrumentation and maintenance costs and introduces privacy concerns.

Alternative approaches not restricted by the LoS requirement include acoustic tracking, where objects instrumented with commodity speakers and microphones can be localized within the environment; Liu et al. present a survey of indoor acoustic localization approaches [33]. However, acoustic approaches can suffer from multipath effects and require careful selection of the frequency bands of the emitter/microphone pair [33]. RF tracking

approaches [42] operate on similar principles and include systems that can localize WiFi [14], BLE [9, 13], or RFID tags [35] within a room. While these systems have decreased resolution compared to optical approaches (i.e., cm-scale vs. mm-scale), they have greater robustness to LoS occlusions but, similar to acoustic approaches, remain sensitive to multipath issues. Fusing these approaches with other sensors, such as IMUs, has also shown increased robustness to LoS issues [8]. As magnetometers with high sensitivity and measuring range become more widely available, magnetic tracking has emerged as a high-resolution and environmentally robust approach [45] to tracking objects by instrumenting them with magnets (either an electromagnet or passive magnet). Section 2.3 below covers these magnetic approaches in greater detail.

2.2 Interactive Surfaces

Making surfaces interactive has generally involved either instrumenting the environment [41] (or users [21]) with sensors to track interactive events, such as with cameras [37], or instrumenting the surface itself [20], such as with contact-based sensors [12]. Instrumenting the environment, rather than the surface of interest directly, offers the advantage of not having to modify each surface a user would wish to interact with individually and often avoids altering the appearance or texture of the surface, such as by applying a coating [50] or sensors onto the surface. However, the distance between the environmental sensor and its target can affect tracking range [35]; for example, depth cameras significantly increase in estimation error with increased distance and largely only maintain depth accuracy $\leq$4 m [1].

Conversely, by directly instrumenting surfaces, sensing approaches can focus on a well-defined area to support a multitude of interactive modalities and take advantage of their fine-grained resolution in addition to tracking touch and recognizing gesture (e.g., human event detection [24]). Additionally, directly instrumenting surfaces offers consistency and robustness to environmental factors that frequently affect approaches that instrument the environment, such as if the interactive surface is moved further away from a sensor, a camera's view is partially occluded, or the introduction of noise sources (e.g., light, sounds, RF waves). MagDesk instruments a surface with 112 magnetometers and enables fine-grained sensing of magnetic objects without affecting the surface's appearance by placing the magnetometer array underneath, such as on the underside of a table. Since most common household surface materials (e.g., wood, quartz) are not ferromagnetic and have a relative magnetic permeability of 1 (i.e., the same as in a free space vacuum [18]), the surfaces are effectively "transparent" to the magnetometer array.

2.3 Magnetic Sensing and Tracking

Magnetic field sensing offers a rich information channel for interactive applications [19, 23]. Within magnetic sensing for tracking, approaches are typically based on tracking active electromagnets or passive permanent magnets. Active electromagnetic sensing approaches, such as Aura [48], AuraRing [40], and Finexus [11], track small electromagnets with a magnetic sensing array. These electromagnets can be driven at a specific frequency, which assists in identifying individual electromagnets and overcoming the Earth's background noise. However, electromagnets do require a power source and supporting driving hardware as opposed to permanent magnets. While MagDesk can support both active and passive magnetic sensing approaches, we primarily present our results using N42-grade passive magnets [36].

Permanent magnets, such as neodymium magnets, create a persistent magnetic field. Systems that employ these magnets can utilize passive tags (i.e., ones that do not require power or maintenance) to enable continuous tracking [46]. For example, MagX [10] tracks fingertip positions without any instrumentation overhead beyond wearing magnetic rings. MagHacker [34] tracks the internal magnet of a digital stylus to infer written text. GaussSense [31] and its subsequent works [27, 29, 30, 32] instrument the backside of portable touchscreen displays with an analog Hall-sensor grid to sense the magnetic field emitted by permanent magnets within stylus

or magnetic widgets, enabling occlusion-free drawing or tangible interactions. However, its tracking capabilities are limited to near-surface (within 50mm of the display), and the system cannot obtain full 3D position and orientation tracking with the magnet at an arbitrary angle. Further, since the magnetic tangibles' locations are determined from pixel coordinates in a magnetic image up-sampled from the sensor grid readings, the tracking resolution is fundamentally limited by the sensor density, making extending up to desk or room-scale unrealistic. To increase sensing range, other approaches have looked towards combining passive magnetic tracking with other sensing modalities through sensor fusion, such as acoustic tracking in MagSound [45], to enable high-resolution tracking at close ranges (e.g., within a meter) while offering reasonable localization at room-scale.

The works discussed above highlight challenges associated with passive magnetic approaches, including achieving long-range capabilities and system scalability (i.e., room-scale tracking). To increase the range capabilities of passive magnetic tracking, MagDesk uses a novel approach to dynamically adjust the position and number of magnetometers used to track the passive magnets and employs an adaptive filter to maintain tracking resolution even at 600 mm and with a sparse magnetometer array (i.e., 100 mm sensor spacing as opposed to 5 mm in GaussSense).

3 System Design & Implementation

The MagDesk sensing platform consists of two functional components: a physical array of 112 magnetometers that measures the magnetic field induced on the surface of the table and a software pipeline that uses the Levenberg–Marquardt (LM) damped least-squares algorithm to solve the vector form of the magnetic dipole model to estimate magnet's location in 3D space. The coordinates are then fed through a multi-parameter adaptive filtering algorithm to accurately and robustly predict the source magnet's location in real-time. This section provides a background on the theory of operation for tracking passive magnets (Section 3.1) and details the hardware (Section 3.2) and software (Section 3.3) implementation of MagDesk, followed by a technical evaluation of tracking performance in Section 4.

3.1 Theory of Magnetic Tracking

MagDesk tracks the movements of permanent magnets by sensing the spatial distribution of the induced magnetic flux density near the table surface. The magnetic field strength around a magnet can be modeled by the dipole model [15], as described by Equation 1:

$$\vec{B} = \frac{\mu_0}{4\pi}\left(\frac{3(\vec{m}\cdot\vec{r})\vec{r}}{|\vec{r}|^5} - \frac{\vec{m}}{|\vec{r}|^3}\right) \tag{1}$$

where μ_0 is the permeability of free space, $\vec{r}$ is the vector from the magnet to the magnetometer's coordinate, and $\vec{m}$ is the magnetic moment, as visualized in Figure 2.

While the magnetic field from any static magnetic source resembles a dipole at a sufficient distance, a spherical magnet's flux density aligns the closest to the dipole model [25], and is thus used for this mathematical analysis. Since the magnetic field strength is symmetric around the axis of the dipole, the magnetic moment $\vec{m}$ can be described in a spherical coordinate system as shown in Figure 2 and mathematically represented in Equation 2:

$$\vec{m} = m\begin{pmatrix}\sin\theta\cos\phi\\ \sin\theta\sin\phi\\ \cos\theta\end{pmatrix} \tag{2}$$

where m is the constant magnitude of the magnetic moment of a passive magnet. Therefore, the 5-DoF pose of a spherical magnet is characterized by the parameters $[x, y, z, \theta, \phi]$. Since the Earth generates a spatially uniform magnetic field, the magnetic field strength measured by each magnetometer can be represented by a linear

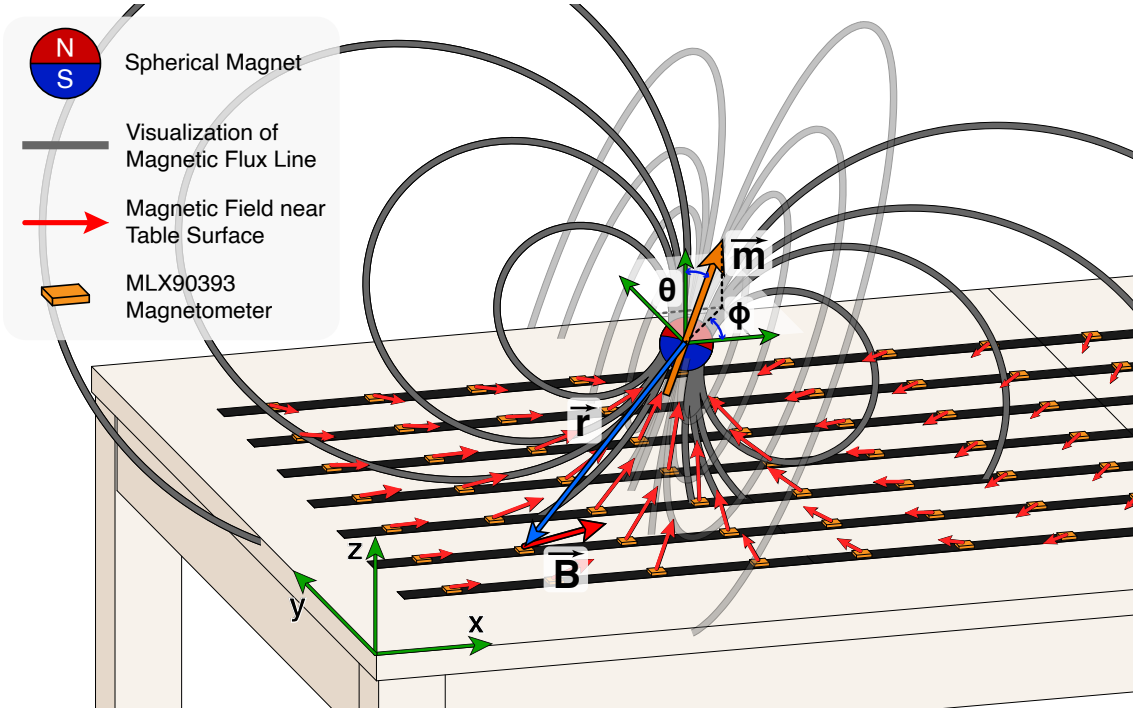

Fig. 2. Demonstration of the magnetic dipole model, visualizing the external magnetic field around a spherical magnet as measured by the magnetometer array. $\vec{B}$ is the magnetic field strength measured by a magnetometer; $\vec{m}$ is the magnetic moment; $\vec{r}$ is the vector from the magnet to the sensor; θ and ϕ are the spherical coordinates in MagDesk's reference frame.

combination of the field produced by each magnet and the Earth's magnetic field. The magnetic field at the ith sensor is given by Equation 3:

$$\vec{B}_i = \vec{G}_i + \sum_{j=1}^{j=M} \frac{\mu_0}{4\pi} \left(\frac{3(\vec{m}_j \cdot \vec{r}_{ij})\vec{r}_{ij}}{|\vec{r}_{ij}|^5} - \frac{\vec{m}_j}{|\vec{r}_{ij}|^3} \right) \tag{3}$$

where $\vec{G}_i$ is the average background magnetic field, $\vec{m}_j$ is the magnetic moment of the jth magnet, and $\vec{r}_{ij}$ is the vector from the jth magnet to the ith magnetometer's coordinate.

MagDesk combines the 3-axis sensor readings from an array of N magnetometers, which results in a series of $3N$ non-linear equations. With the magnitude of magnetic moment and background magnetic field known, tracking M magnets requires solving for $5M$ parameters. To solve these equations efficiently, a real-time *analytical solver* was developed using the Levenberg-Marquardt (LM) algorithm, an iterative optimization algorithm based on gradient descent [39]. By providing an initial estimate of the magnet's pose, i.e., a *seed point*, and the Jacobian matrix at that location, the algorithm generates an optimal magnet pose that minimizes the differences between the magnetometer readings and the magnetic field distribution predicted by the dipole model.

While the analytical solver provides an accurate prediction of magnet poses when the strength of the induced magnetic field is strong near the table surface, the tracking performance deteriorates when the magnet is higher above the table, as the magnetic field strength of a dipole degrades with the cube of the distance $\vec{r}_{ij}$. If the magnitude of the measured magnetic field, i.e., excluding the Earth's background, approaches the standard

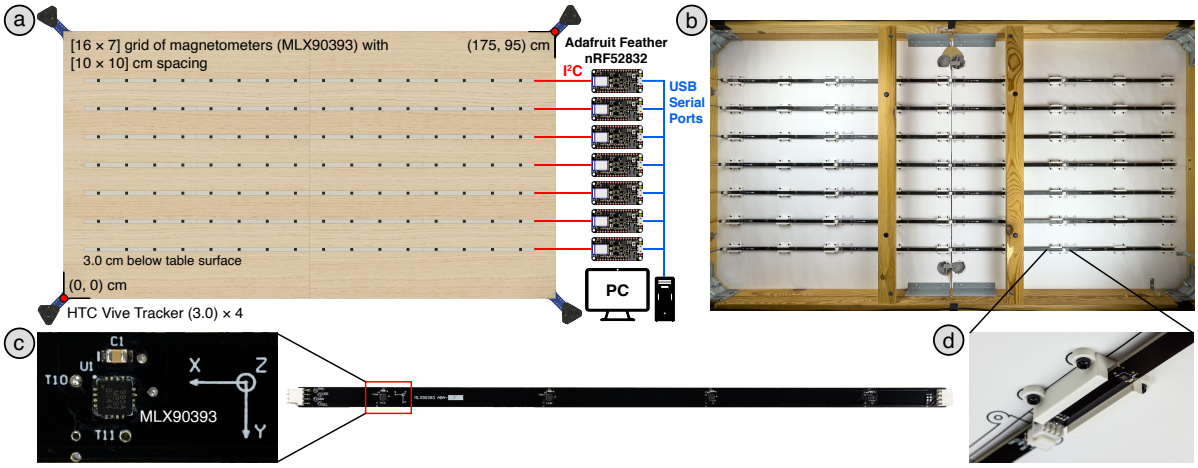

Fig. 3. (a) Hardware schematic of MagDesk, showing the magnetometer array and data flow. (b) Sensor PCBs installed underneath the tabletop using 3D-printed fixtures. (c) Chainable PCB with the zoomed-in view of the MLX90393 magnetometer. (d) 3D-printed PCB holder positioning the magnetometers 3 cm beneath the table surface.

deviation of magnetometer reading noise, the LM algorithm will not be able to closely align the magnet pose prediction to the measurement, resulting in poor tracking performance. An unstable solver prediction has two consequences: (1) low tracking accuracy; (2) if an inaccurate prediction that deviates significantly from the ground truth is used as the seed point for the next iteration, the solver might converge to an incorrect local minimum for the magnet pose and the tracking would be lost.

To address these limitations of the LM algorithm, MagDesk adopts a filtering pipeline after the solver prediction based on two observations: (1) the magnet usually follows a smooth and continuous path during user interactions; (2) averaging magnet poses over consecutive predictions improves tracking performance during user interactions (e.g., the speed of the magnet is bounded by human performance, and the magnet can not teleport across the table). The implementation details of the filtering pipeline are described in Section 3.3.3.

3.2 Hardware Implementation

MagDesk consists of a 175 × 95 cm wooden desk retrofitted with an array of 112 commercial-off-the-shelf, low-cost magnetometers (MLX90393) underneath the surface [38]. As shown in Figure 3a, the magnetometers are arranged in a 7-row × 16-column grid at the center of the table with 10 cm horizontal spacing between adjacent sensors, which balances the implementation complexity and sensing resolution. To aid in deployability and system wiring, 40 cm-long printed circuit boards (PCBs) were designed consisting of 4 magnetometers spaced 10 cm apart. Connectors on both ends route power and data, allowing strips of magnetometers to be easily constructed, reconfigured, and swapped out as needed. For this installation, 3D-printed brackets were designed to hold the PCBs in place, and the long strips of PCBs were placed 10 cm apart, as shown in Figure 3. The instrumentation approach described above allows the magnetometer array to be reconfigured and expanded underneath any regular surface. An Adafruit Feather nRF52832 module [4] collects 3-axis sensor readings from the 16 magnetometers in a row at 32.1 Hz through an I2C bus with 400 kHz clock frequency. Each sensor in a row has a unique I2C address. In the current setup, seven Arduino Feather boards stream the readings to a PC through USB serial ports.

3.3 Software Implementation

3.3.1 Overview of Software Design. The software design of MagDesk consists of an initialization phase and a sensing loop. During the initialization, the computer handshakes with the 7 Adafruit Feather boards to establish serial communication, and the array of magnetometers is configured through the I2C bus. Then, the system collects the background magnetic field at each sensor location for 10 seconds without the magnetic objects that will be tracked directly on the tabletop. It should be noted that while the Earth's magnetic field is relatively stable, minor natural fluctuations do occur on the time scales of days and weeks, and thus, periodic calibration is needed. Additionally, static (non-moving) magnetic and ferromagnetic objects on the table surface, such as monitors and keyboards, can be accounted for in the calibration process, reducing the user's burden. Next, the program initializes the magnet pose to a pre-defined seed position for the analytical solver, e.g., on the surface at the center of the table. When the user brings the magnet close to the seed position, e.g., within 20 cm, the solver will converge to the magnet's position and orientation, after which the magnet will be tracked continuously through the sensing loop.

In the sensing loop, the user moves the magnet-embedded objects to interact with the UI. Then, the magnetometer array measures the magnetic fields at 112 sensor locations and subtracts the Earth's background (and any static magnetic field). The inputs to the analytical solver are updated based on the readings and the magnet's previous pose. The solver is executed, after which the filtering pipeline combining a Kalman filter and a moving average filter with adaptive filtering parameters is applied. If the solver converges, e.g., the prediction is within 20 cm of the seed position, the sensing loop continues; otherwise, the system loses track of the magnet, and the user is prompted to reset the magnet to the initial seed position to reacquire tracking. While tracking loss has the potential to disrupt user experience, loss of tracking is rare, as will be shown in Section 6, and the system is robust enough to enable diverse and complex real-time user applications. The sensing loop completes within the duration of magnetometer data collection, maintaining the 32.1 Hz refresh rate for the entire array of 112 magnetometers. For reference, Figure 18 in the Appendix visualizes MagDesk's software design. Note that the process above describes the procedures of tracking a single magnet – multi-magnet tracking will be discussed in Section 4.3.3.

3.3.2 Analytical Solver. To determine the poses of permanent magnets, MagDesk leverages an analytical solver executing the LM algorithm, which solves non-linear least squares problems based on gradient descent [39]. Since the magnetic characteristics of spherical magnets can be accurately described by the dipole model, the LM algorithm provides benefits over data-driven machine learning (ML) approaches for its faster execution speed and adaptability to different magnet shapes and sizes without excessive training data. While machine learning could be used for noise reduction and clustering functions, similar to the usage in imaging applications, the ML model has to be retrained for different magnets and sensor configurations. Furthermore, the underlying mathematical model of a dipole magnet has been thoroughly examined and verified by the physics community, and it is unlikely that a learning approach can outperform the mathematical model. For MagDesk, the LM algorithm was implemented in C++ using the Ceres Solver library, a speed-optimized non-linear solving library [5]. The C++ implementation is exported using pybind11, allowing the function to be invoked by the MagDesk software pipeline written in Python [26]. At each iteration of sensor reading updates, the solver uses the predicted magnet pose in the previous cycle as the seed point, i.e., an initial estimate of the magnet's state. Using the magnetometer readings, sensor positions, and the previous 5-DoF coordinates of the magnet as inputs, the solver function generates a new prediction of magnet pose.

3.3.3 Adaptive Filtering Pipeline. To compensate for inaccurate prediction when the signal-to-noise ratio (SNR) between measured magnetic fields and sensor noise is low, MagDesk implements a filtering pipeline on top of the analytical solver, combining a Kalman filter and a windowed moving average filter. The Kalman filter

is applied to the output of the LM algorithm for smoothing the tracking path, while the moving average filter suppresses high-frequency noises in the filter prediction [7]. However, a fixed set of parameters for the Kalman and averaging filter is suboptimal as the expected prediction error varies with tracking heights, magnet sizes, and estimated speeds. The same magnet incurs a larger error at higher heights above the table as the SNR decreases. Compared to a smaller magnet, a larger one with a stronger dipole moment results in lower errors at the same height. To tackle a large tracking error, when the magnet moves slowly, the estimated poses could be averaged over a longer time frame, further improving the tracking performance. Note that the delay resulting from the moving average would degrade tracking performance when the magnet moves fast. Therefore, MagDesk adopts an *adaptive* filtering pipeline, the schematics of which are visualized in Figure 19 in the Appendix.

During the preparation phase, for each magnet size, the average stationary position and angle measurement errors at various heights are measured and extracted with 5 cm intervals. Then, cubic interpolation is performed between error values at 5 cm increments. In each iteration, the analytical solver predicts the unfiltered magnet height h_t. Next, the average position and angle measurement errors Err_t at height h_t are estimated using the cubic interpolation. The *measurement* noise of the Kalman filter is updated based on the estimated average tracking error, i.e., different variances for position (3-DoF) and orientation (2-DoF), after which the Kalman filter is applied. Then, the current linear and angular speeds v_t are estimated using the last 0.6 sec of the predicted tracking path. More specifically, the magnet poses between $[t, t-0.3]$ and $[t-0.3, t-0.6]$ are averaged to minimize prediction noise, and the subtracted displacement is divided by a 0.3 sec time duration to estimate the instantaneous speed v_t. Next, the window size of the averaging filter is updated based on the estimated magnet speed v_t and average measurement error Err_t. The window size is capped at 0.5 sec to limit the maximum delay, i.e., $\Delta t = max(Err_t/v_t, 0.5)$. The program applies the moving average filter with the updated window size and updates inputs to the analytical solver for the next iteration.

The improvement of the adaptive filtering pipeline over the raw outputs from the LM algorithm is discussed in Section 4.2.2. The filtering parameters and tracking performance for various magnet sizes are discussed in Section 4.3.2.

4 Technical Evaluation

To evaluate the tracking accuracy of the analytical solver and adaptive filtering pipeline, a benchmarking tool was developed to compare the magnet pose prediction to the ground truth measurement. In the following sections, Section 4.1 describes the hardware setup for technical evaluation; Section 4.2 presents the tracking performance for a single magnet; Section 4.3 explores a few experiments on the effects of (1) magnet movements, (2) magnet sizes, (3) magnet separations, and (4) magnetometer array density on the tracking performance.

4.1 Experiment Setup

To evaluate the tracking performance of MagDesk, a benchmarking tool was developed using the HTC Vive system with individual Vive Trackers (3.0) attached to the magnets as ground truth references [17]. To construct a reference frame with respect to MagDesk, a Vive Tracker was attached to each of the four corners of MagDesk using 3D-printed stands, shown in Figure 4c. Four SteamVR Base Station 2.0, which emit a pattern of infrared light, were placed around MagDesk as lighthouses for inside-out tracking. To rigidly affix the spherical magnets to Vive Trackers, 3D-printed attachment tools were designed for various magnet sizes, as shown in Figure 4a.

For all magnet sizes, the centroid of the magnet, i.e., the center of the magnetic dipole, was positioned 100 mm away from the tracker's origin, with the magnet's north pole aligning to the tracker's z-axis. Figure 4b shows the assembled attachment tool with a 3/4"-diameter magnet.

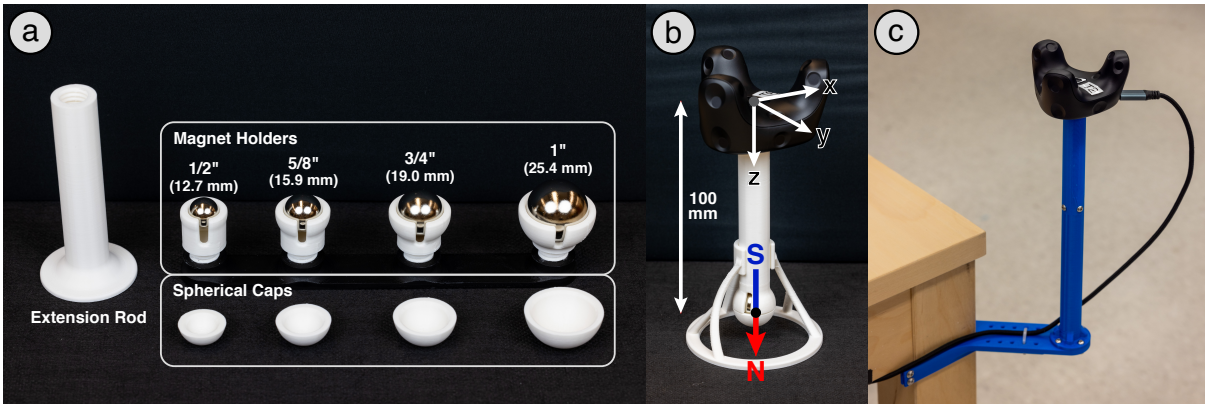

Fig. 4. (a) 3D-printed attachment tools for four magnet sizes: 1/2", 5/8", 3/4", and 1" diameter. (b) Assembled testing device with a 3/4"-diameter magnet attached to a Vive Tracker. (c) Vive Tracker attached to the table corner using a 3D-printed stand to correlate Vive's reference frame with MagDesk's.

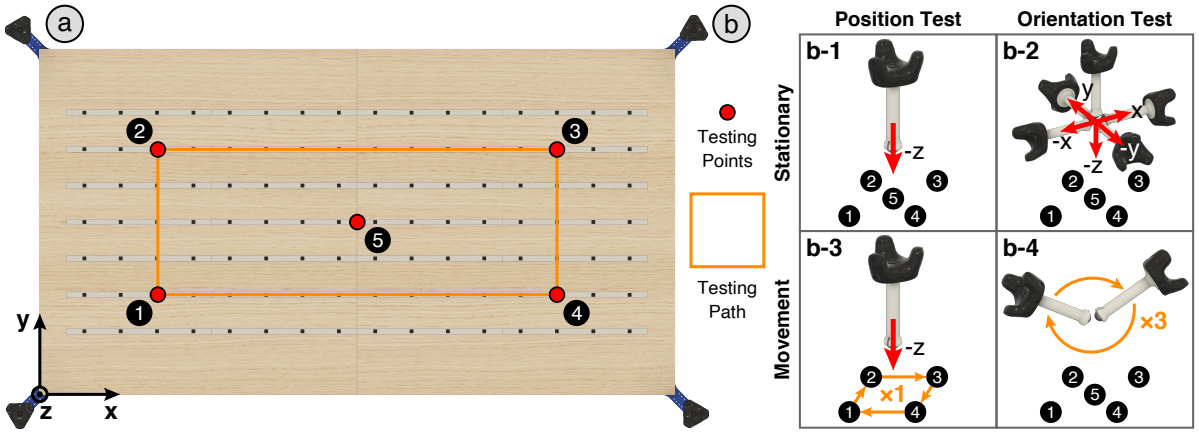

Fig. 5. (a) Selected testing locations and path for evaluating MagDesk's tracking performance. (b) Magnet locations and poses for evaluating the position and orientation accuracy when the magnet is stationary and in motion.

4.2 Single-Magnet Tracking Performance

4.2.1 Evaluation Methods. To determine MagDesk's accuracy in tracking a single object, a 3/4 in. (19 mm)-diameter spherical magnet was selected as the baseline condition. With the Vive Tracker attached, the magnet was positioned at five predetermined locations above MagDesk, as indicated in Figure 5a. To evaluate the 3D *position* accuracy, the magnet was held stationary at each of the five locations with its magnetic dipole pointing downward perpendicular to MagDesk (Figure 5b-1). To evaluate the *orientation* accuracy, the magnet was fixed stationary at points 1 - 5 with its north magnetic pole pointing towards [−z, -x, y, x, -y] in MagDesk's reference frame, as visualized in Figure 5b-2. The tracking performance was evaluated at various heights above MagDesk every 5 cm. For each height, testing location, and magnet orientation, the 3-axis sensor readings from 112 magnetometers and the ground truth poses from the Vive Tracker were collected for 5 seconds. i.e., around 160 samples.

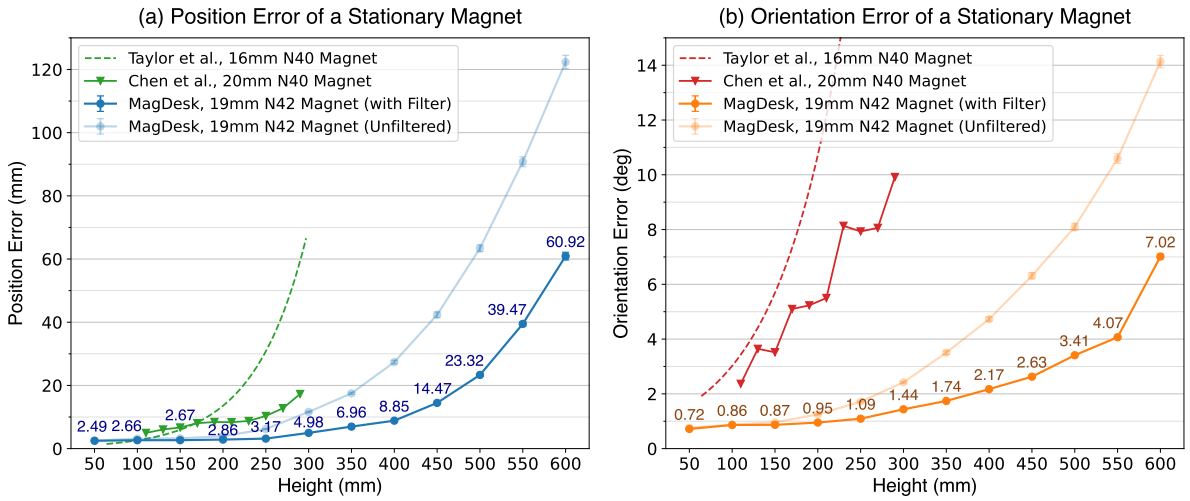

Fig. 6. Positional (a) and orientational (b) error of tracking a stationary magnet for heights up to 600 mm, compared with results from prior works. Both the raw outputs from the analytical solver and the improved results after applying the adaptive filtering pipeline are presented.

After the measurements were collected, for each 5-second group of data, an analytical solver was invoked with the predicted pose from the previous cycle being used as the seed point for the subsequent iteration, achieving continuous tracking. For each sample, the position error is calculated by subtracting the predicted 3D coordinates from the ground truth. The orientation error is derived from the angle between the 3D vectors formed by the predicted north magnetic pole and the Vive Tracker's z-axis. The average stationary position and angle measurement errors based on the *unfiltered* solver prediction were calculated at each height and interpolated, as shown in the preparation phase of the adaptive filtering pipeline (Figure 19b in the Appendix). With the Kalman filter and moving average filter updated with the unfiltered position and angle errors of the particular magnet size, the analytical solver was executed again on all collected magnetometer readings with the adaptive filtering pipeline. Then, the improved position and orientation tracking accuracy were recalculated.

4.2.2 Evaluation Results. The position and orientation errors of tracking a single magnet are plotted in Figure 6, along with results from prior works. The annotated values show the tracking performance with the adaptive filtering pipeline. Each data point represents approximately 800 samples for position error and 2500 samples for orientation error. Compared with the raw outputs from the analytical solver, the filter decreases the average position error by 56.2% and orientation error by 51.3% across all heights. Near the table surface, MagDesk achieves positional and orientational accuracy of *2.49 mm* (SD: *0.47 mm*) and *0.72 deg* (SD: *0.38 deg*), respectively. The maximum trackable height reaches 600 mm while maintaining stable and continuous tracking, with an average position and orientation error of *14.40 mm* (SD: *12.28 mm*) and *2.25 deg* (SD: *1.69 deg*) across the entire sensing range. Compared with prior works [10, 44] that explored 3D tracking of permanent magnets, MagDesk provides a longer sensing range and higher tracking accuracy. Within the 300 mm tracking range demonstrated in prior works, MagDesk achieves average positional and orientational error of *3.14 mm* (SD: *1.52 mm*) and *0.99 deg* (SD: *0.53 deg*), performances suitable for fine-grained interactive applications. For an intuitive visualization of the tracking performance, the ground truth and predicted magnet positions and orientations collected during the evaluation are visualized for every 10 cm height in Figure 20a-b in the Appendix.

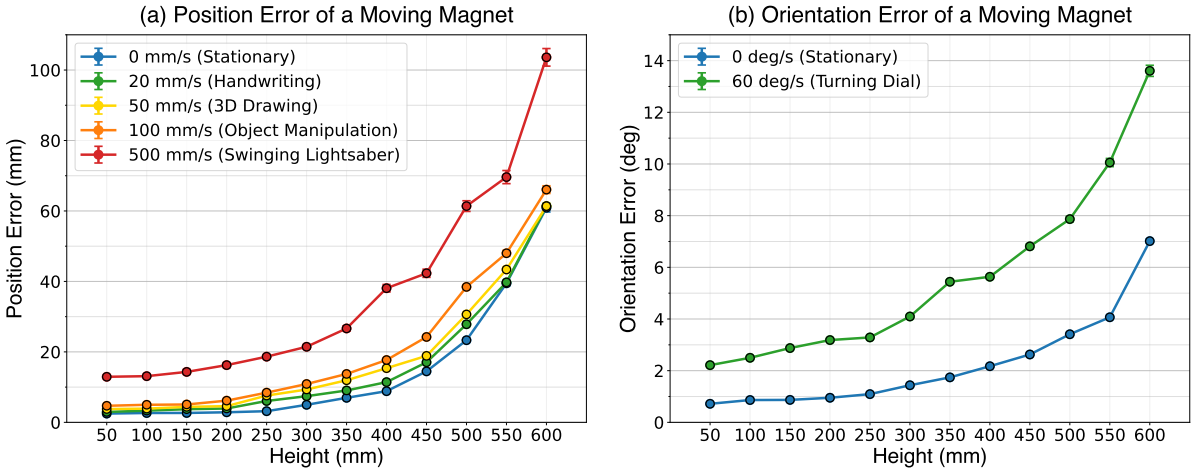

Fig. 7. Positional (a) and orientational (b) error of tracking a magnet moving at various speeds for heights up to 600mm.

Error Type	Magnet Speed	Average Error across Sensing Range	Error Increase compared to Stationary	Improvement by Filtering Pipeline
Position	0 mm/s	14.40 mm (SD: 12.28 mm)	0%	56.2%
Position	20 mm/s	16.16 mm (SD: 13.68 mm)	12.2%	51.2%
Position	50 mm/s	17.93 mm (SD: 13.48 mm)	24.5%	46.5%
Position	100 mm/s	20.70 mm (SD: 13.74 mm)	43.7%	39.9%
Position	500 mm/s	36.53 mm (SD: 22.00 mm)	153.7%	11.8%
Orientation	0 deg/s	2.25 deg (SD: 1.69 deg)	0%	51.3%
Orientation	60 deg/s	5.63 deg (SD: 3.79 deg)	150.6%	14.8%

Table 1. Summary of the average position and orientation error across the entire sensing range for a moving magnet.

4.3 Tracking Experiments

The following sections describe several experiments to quantify the localization performance of MagDesk for (1) a magnet in motion, (2) magnets of different sizes, (3) multiple magnets, and (4) sparser magnetometer array density.

4.3.1 Effects of Magnet Movements. To demonstrate MagDesk's usability as a tracking platform for user interactions, its tracking performance while the magnet moves at various speeds was evaluated. Four translation speeds were selected, with corresponding scenarios in 3D VR/AR applications: *20 mm/s* (handwriting), *50 mm/s* (3D drawing), *100 mm/s* (object manipulation), and *500 mm/s* (swinging lightsaber). One rotation speed, *60 deg/s*, which corresponds to turning a dial, was evaluated. For translation movement, the assembled 3/4"-diameter magnet and Vive Tracker were moved along the testing path indicated in Figure 5a with the magnetic dipole pointing downward perpendicular to MagDesk (Figure 5b-3). For rotation movement, the magnet was rotated horizontally around each of the five test points for three revolutions in a 3D-printed holder (Figure 5b-4).

The position and orientation errors are plotted in Figure 7, along with results from the stationary measurement. Table 1 summarizes the results for each magnet speed, including the average tracking error across the 600 mm sensing range, the increased error compared to a stationary magnet, and the improvements by the filtering pipeline

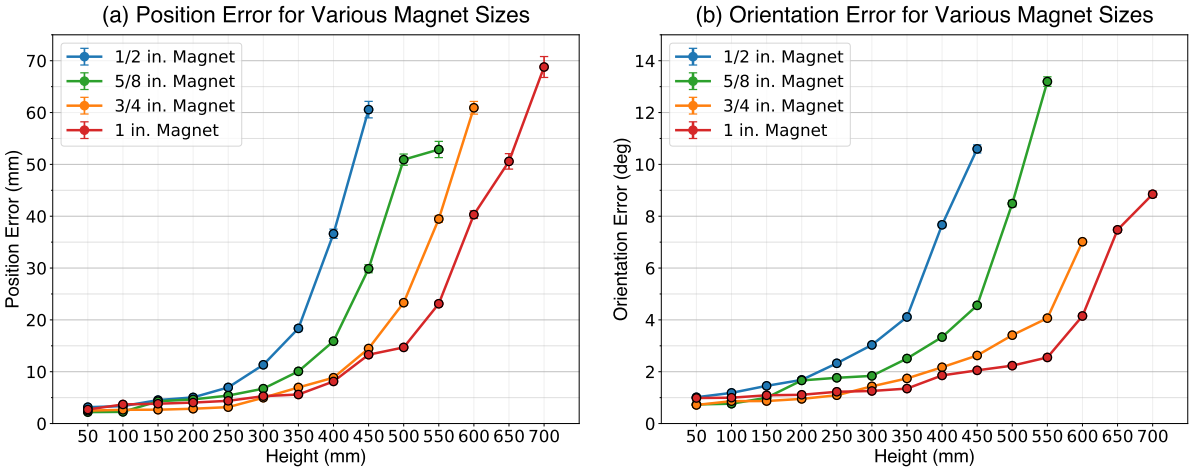

Fig. 8. Positional (a) and orientational (b) error of tracking magnets of various sizes. For each magnet, the errors are plotted up to their maximum trackable range.

Error Type	Magnet Diameter	Tracking Range	Average Error across Sensing Range	Average Error up to 450 mm	Improvement by Filtering
Position	1/2"	450 mm	16.66 mm (SD: 14.31 mm)	16.66 mm (SD: 14.31 mm)	51.5%
Position	5/8"	550 mm	16.83 mm (SD: 14.93 mm)	9.04 mm (SD: 7.22 mm)	54.9%
Position	3/4"	600 mm	14.40 mm (SD: 12.28 mm)	5.46 mm (SD: 3.67 mm)	56.2%
Position	1"	700 mm	17.74 mm (SD: 16.59 mm)	5.66 mm (SD: 2.64 mm)	24.1%
Orientation	1/2"	450 mm	3.67 deg (SD: 3.23 deg)	3.67 deg (SD: 3.23 deg)	47.5%
Orientation	5/8"	550 mm	3.62 deg (SD: 3.39 deg)	2.02 deg (SD: 1.51 deg)	45.4%
Orientation	3/4"	600 mm	2.25 deg (SD: 1.69 deg)	1.39 deg (SD: 0.86 deg)	51.3%
Orientation	1"	700 mm	2.66 deg (SD: 2.23 deg)	1.32 deg (SD: 0.83 deg)	25.5%

Table 2. Summary of the average position and orientation error for spherical magnets of various sizes.

compared to the raw solver predictions. The results suggest that the filtering pipeline is effective at reducing tracking errors for various speeds and that the tracking performance is adequate for interactive applications, even for fast-moving objects. Note that at lower heights, i.e., below 300 mm, the larger position errors for 500 mm/s speed are mainly attributed to the delay resulting from the 32.1 Hz update rate (31.2 ms duration). For below 300 mm, the average position error is *3.14 mm* for a stationary magnet and *16.12 mm* for a magnet moving at 500 mm/s. The *12.98 mm* difference corresponds to a 26.0 ms delay for 500 mm/s movement speed, matching the delay resulting from the update rate. For an intuitive visualization of the tracking performance, the ground truth and predicted magnet positions and orientations collected during the tracking experiments are visualized for every 10 cm height in Figure 20c-d in the Appendix.

4.3.2 Effects of Magnet Sizes. According to the dipole model, the spatial distribution of magnetic flux density around a spherical magnet is solely characterized by the strength of its dipole moment. With known magnitudes of dipole moments, MagDesk's analytical solver can accurately determine the pose of magnets of various shapes and sizes. A larger magnet with a stronger dipole moment has a higher SNR as measured by the magnetometer

array, resulting in a lower prediction error and longer tracking range. Conversely, while a smaller magnet with a weaker dipole moment has a limited tracking range, its compact size and lower weight allow it to be integrated into daily objects more discreetly. To determine the effects of magnet sizes on tracking performance, the evaluations in Section 4.2.1 were repeated for N42-grade spherical magnets of three other sizes (1/2 in., 5/8 in., and 1 in. diameter), the specifications of which are listed in Table 6 in the Appendix with the baseline magnet size highlighted.

The position and orientation errors of tracking magnets of four sizes are plotted in Figure 8 up to their respective maximum trackable range. Table 2 summarizes the results for each magnet size, including its maximum tracking height above the table surface, the average error across its entire sensing range and up to 450 mm, and the improvements by the filtering pipeline. The results indicate that the maximum trackable height increases with the magnet size, with the largest 1" magnet achieving a 700 mm range. At the same height, a larger magnet generally has lower tracking errors, and the dependency is more significant at higher heights, i.e., above 300 mm, as shown in Figure 8. The average errors up to 450 mm listed in Table 2, i.e., the maximum range attained by the smallest 1/2" magnet, also validate this trend. The results also suggest that the filtering pipeline is effective at reducing tracking errors for different magnet sizes and dipole strengths. In summary, to achieve the maximum sensing range, an interactive application should choose a larger magnet as the tracker. Note that the 64.4 g weight of the heaviest 1" magnet (Table 6 in the Appendix) is still lighter than a typical VR tracker, e.g., the Vive Tracker (3.0) weighs 75 g and requires a rechargeable battery. On the other hand, for applications that demand less tracking range but are space-constrained, a smaller magnet could be used. Even the smallest 1/2" magnet weighing 8.05 g achieves 5 mm position accuracy and 2 deg orientation accuracy up to 200 mm.

4.3.3 Multi-Magnet Tracking. The expansive surface area of MagDesk provides opportunities for simultaneous multi-object tracking. While multiple spherical magnets could be tracked individually by segmenting the magnetometer array into regions, the magnetic field distributions surrounding the magnets overlap and disturb each other when two magnets are in close proximity. To evaluate the effects of magnet separations on tracking performance, an experiment was conducted with two 5/8"-diameter magnets. The two magnets, each attached to a Vive Tracker, were moved randomly near the MagDesk surface, i.e., within 100 mm, while being rotated simultaneously, and the magnetometer readings and ground truth poses from the two trackers were collected for 10 minutes. The two magnets were brought as close to each other as possible without being physically attracted. After the measurements were collected, an analytical solver was invoked for each magnet, denoted as the *one-magnet solver*. For a 5/8" magnet, the maximum tracking range of 550 mm, as indicated by Table 2, suggests that the magnetic field at more than 600 mm away from it is indistinguishable from the background noise. Therefore, to minimize the disturbance to the sensor readings caused by a nearby magnet, only the magnetometers within a 300 mm horizontal radius are used for each one-magnet solver, instead of the entire magnetometer array.

The position and orientation errors with the one-magnet solver are visualized in Figure 9 as the solid lines. The plot suggests that the average errors start to increase after the magnets are brought to within approximately 400 mm of each other, as indicated by the dashed green line. The maximum position error peaks at around 80 mm separation, which roughly corresponds to the 100 mm spacing between adjacent magnetometers. Within the 100 mm sensor spacing, the analytical solver is unable to resolve the magnetic field of individual magnets and has a higher chance of identifying the two magnets as one. This could be verified by the slight drop in position error between 80 mm and 30 mm, i.e., the average error is around 35 mm when the two magnets are 30 mm apart.

To improve the tracking performance when two magnets are close together, MagDesk adopts an analytical solver that simultaneously tracks two magnets, i.e., the *two-magnet solver*. This alternative solver accepts the poses from both magnets as seed points and predicts two sets of 5-DoF position and orientation information. The analysis was re-executed with the new solver using the readings from the entire magnetometer array, the results of which are visualized in Figure 9 as the dashed lines. The plot suggests that the two-magnet solver has

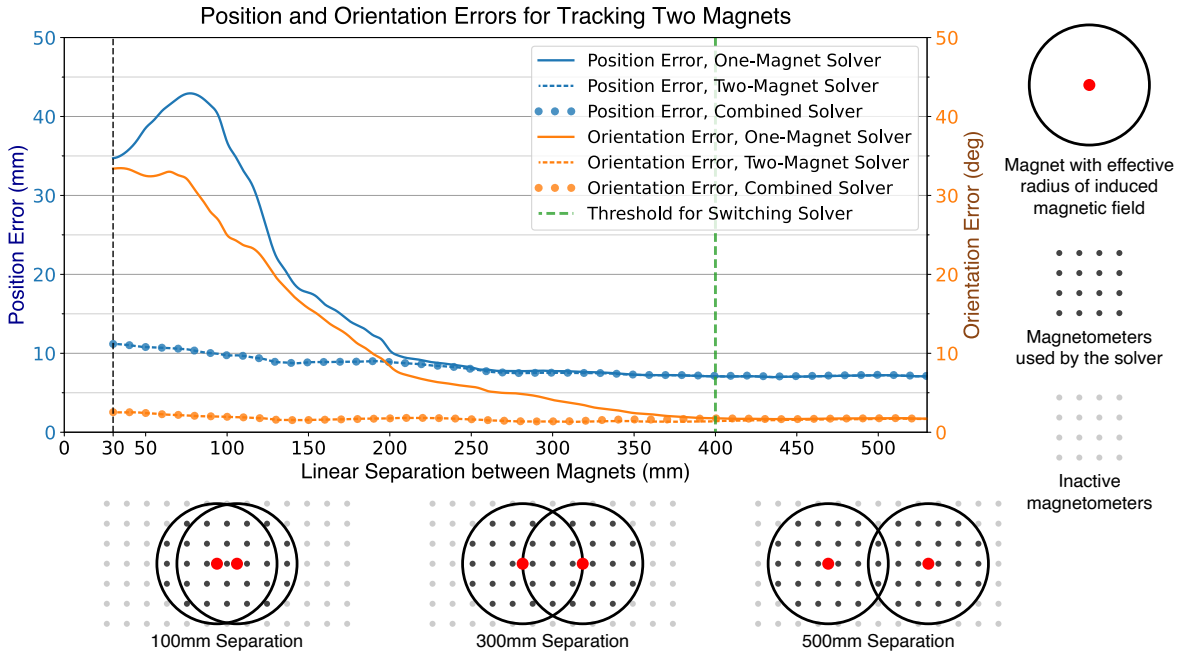

Fig. 9. The average positional and orientational errors of tracking two 5/8"-diameter magnets using the one-magnet, two-magnet, and combined solver when they are spatially separated by various distances.

Magnet Size	Horizontal Radius	Threshold Distance
1/2"	250 mm	350 mm
5/8"	300 mm	400 mm
3/4"	350 mm	450 mm
1"	400 mm	500 mm

Table 3. The range of magnetometers used by magnets of various sizes for multi-magnet tracking and the threshold for switching between one- and two-magnet solvers.

indistinguishable performance compared to the one-magnet solver for distances beyond 400 mm while improving the accuracy substantially at closer distances. The solver achieves average positional and orientational accuracy of *11.18 mm* and *2.54 deg*, respectively, even if the two magnets are as close as 30 mm apart.

To allow MagDesk to track an arbitrary number of magnets, a *combined solver* was implemented that automatically switches between the two types of solvers when a threshold distance is crossed. The threshold is set to 400 mm for 5/8" magnets. The performance of the combined solver is visualized as the dotted lines in Figure 9. Its accuracy closely aligns with the two-magnet solver at smaller linear separations while providing flexibility with the number of trackable magnets on the table. With the combined solver, when there are multiple magnets, MagDesk automatically segments the magnetometer array into regions based on a set *horizontal radius* around each magnet depending on the strength of its dipole moment, i.e., a stronger magnet will affect sensors within a larger area. When two magnets of the same size are brought within a *threshold distance*, the algorithm merges

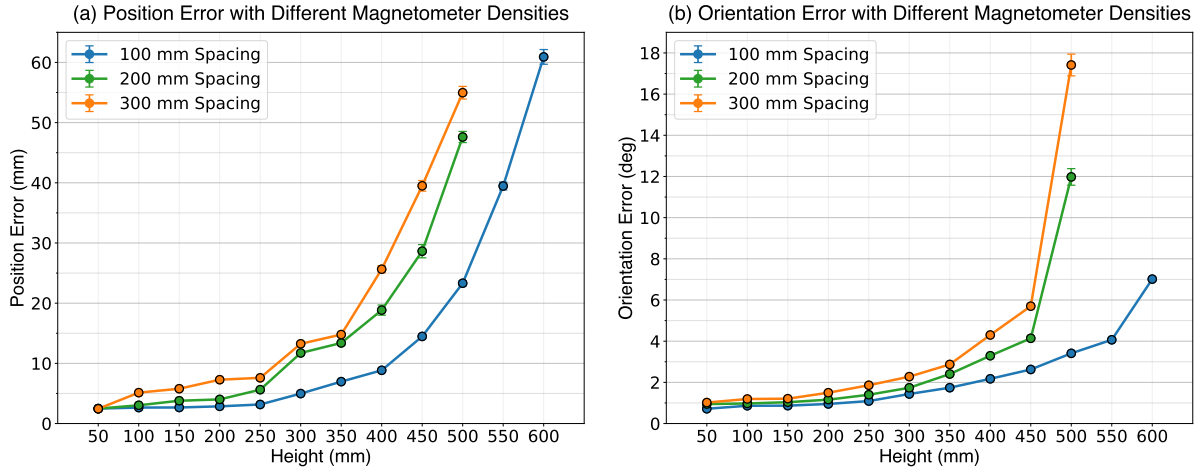

Fig. 10. Positional (a) and orientational (b) error of tracking a stationary magnet with different magnetometer array densities. For each density, the errors are plotted up to the corresponding maximum trackable height.

Magnetometer Spacing	Sensor Array Density	Tracking Range	Error Type	Average Error across Sensing Range	Maximum Height for **20 mm** or **2 deg** Average Error
100 mm	9.29 / ft^2	600 mm	Position	14.40 mm (SD: 12.28 mm)	550 mm
			Orientation	2.25 deg (SD: 1.69 deg)	550 mm
200 mm	2.32 / ft^2	500 mm	Position	13.91 mm (SD: 12.31 mm)	450 mm
			Orientation	2.91 deg (SD: 2.51 deg)	450 mm
300 mm	1.03 / ft^2	500 mm	Position	17.64 mm (SD: 14.56 mm)	400 mm
			Orientation	3.93 deg (SD: 3.27 deg)	400 mm

Table 4. Summary of the average position and orientation error for various magnetometer array densities.

the set of magnetometers affected by both magnets and invokes a two-magnet solver instead. Table 3 shows the *horizontal radius* and *threshold distance* for four magnet sizes.

4.3.4 Magnetometer Array Density. The magnetometer array employed by MagDesk has a 10 cm horizontal spacing between adjacent sensors. Prior works [10] demonstrate that a denser sensor array results in higher tracking accuracy for magnetic sensing. To evaluate the effects of magnetometer array density on tracking performance, the measurements collected in Section 4.2.1 for the 3/4"-diameter magnet were re-analyzed with two sparser sensor densities. i.e., 20 cm and 30 cm spacing. Only a subset of magnetometers were used as inputs to the analytical solver, i.e., 32 magnetometers for 20 cm spacing and 18 magnetometers for 30 cm spacing.

The position and orientation tracking errors with various magnetometer densities are plotted in Figure 10. Table 4 summarizes the results for each array density, including its maximum tracking height above the table surface, the average error across its entire sensing range, and the maximum height while maintaining *20 mm* and *2 deg* average accuracy. Figure 10 indicates that the maximum trackable height and the average accuracy at each height decrease with sparser array densities. However, even with the sparser 200 mm and 300 mm sensor spacing, MagDesk still achieves a 500 mm tracking range, a minor decline compared to the 600 mm baseline. The maximum

Tangible Primitive	Number of Magnets	Magnet Size	Tracking DoF	Output Type	Output Range
Stylus	1	3/4"	3D position + 2D angle	Binary	On/Off
Button (momentary)	1	5/8"	2D position	Binary	On/Off
Button (toggle)	1	5/8"	2D position	Binary	On/Off
Switch	2	5/8"	2D position + 1D angle	Binary	On/Off
Slider	2	5/8"	2D position + 1D angle	Numerical	0 - 300 mm
Knob (absolute)	1	5/8"	2D position	Numerical	-180° - +180°
Knob (relative)	2	5/8"	2D position + 1D angle	Numerical	-180° - +180°
Hinge	2	5/8"	2D position + 1D angle	Numerical	-180° - +180°

Table 5. Summary of the eight primitives for tangible interactions.

height below which MagDesk maintains a *20 mm* average positional accuracy and *2 deg* average orientational accuracy is 550 mm for the default density, 450 mm for 200 mm spacing, and 400 mm for the sparsest 300 mm spacing. Note that even with the 300 mm spacing and 1/9 of the magnetometers, MagDesk attains *10 mm* position accuracy and *2 deg* orientation accuracy up to 250 mm (Figure 10). With approximately one magnetometer per square foot ($1.56 each at 100 units), MagDesk's sensing approach provides an expandable and low-cost solution for accurate 3D object tracking for areas scalable up to room- or warehouse-size.

5 Tangible Interactions

With the 3D tracking capabilities provided by MagDesk, a set of *eight* tangible primitives was designed with one or two spherical magnets embedded in 3D-printed gadgets to enable tangible interactions.

5.1 Design of Tangible Primitives

The eight tangible primitives are listed in Table 5, including the number and size of the magnets and the type and range of their outputs. The tangibles with two magnets employ the two-magnet analytical solver introduced in Section 4.3.3. The stylus uses a 3/4" magnet and provides full 3D position and 2D orientation tracking. The other primitives use 5/8" magnets and provide 2D position tracking near the MagDesk table surface with an additional horizontal angle for devices with two magnets. All magnets are affixed to the tangibles through the attachment tools shown in Figure 4a. The image of the eight tangible primitives is shown in Figure 11a, while their operations are shown in Figure 11b.

Stylus (Figure 11a-1, b-1) The stylus utilizes a 3/4"-diameter magnet attached to a 3D-printed stem with its north pole oriented parallel to the stylus and pointing toward the tip. A cone encapsulates the magnet with a vertex 20 mm away from the magnet's center. A spring-loaded protrusion is positioned at the end of the stylus 110 mm from the magnet's center, which simulates the function of an eraser.

Button - momentary (Figure 11a-2, b-2) The momentary button contains a 5/8" magnet in its spring-loaded upper compartment, with a 15-mm vertical travel distance. When the button is depressed for more than 10 mm, an ON input will be registered (Figure 11b-2[2]). When the button is released, the spring will extend the button to its original state, registering an OFF signal (Figure 11b-2[3]).

Button - toggle (Figure 11a-3, b-3) The toggle button is similar to the momentary button but with the addition of a locking mechanism. When the user twists the upper part counter-clockwise after the button is fully depressed, the button will be locked to its ON position under the force of the spring (see Figure 11b-3 inset). The reverse motion will unlock the button and return it to the original state.

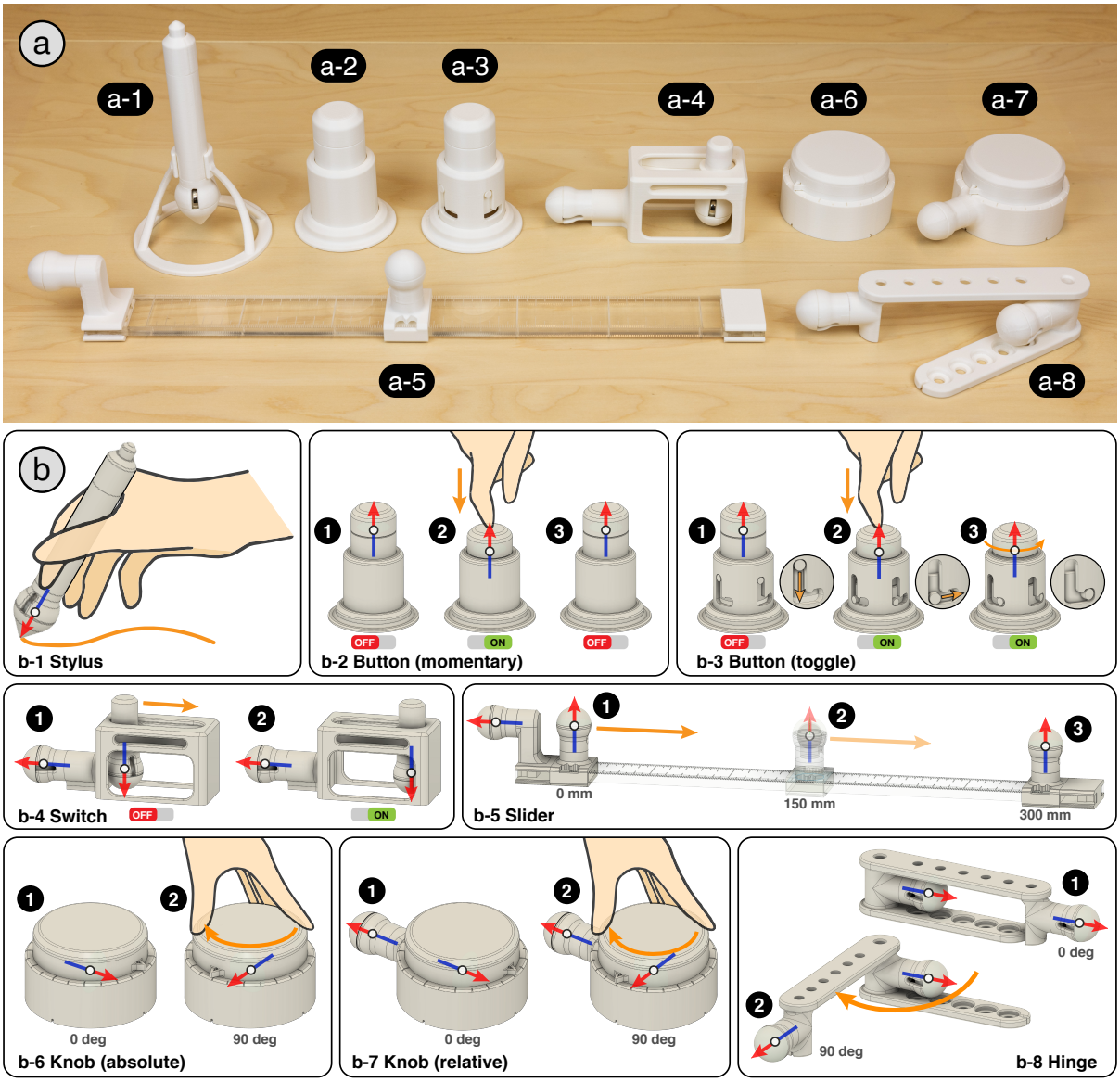

Fig. 11. (a) Image of the eight 3D-printed tangible primitives; (b) Schematics of the tangibles demonstrating their operations, with the polarity of the embedded spherical magnets highlighted.

Switch (Figure 11a-4, b-4) The switch is a binary input device that detects the relative positions of two 5/8" magnets instead of the absolute height of a single magnet, as in the case of buttons. The distance between the two magnets ranges from 50mm (Figure 11b-4[1]) to 90mm (Figure 11b-4[2]). An ON input will be triggered when the movable magnet is slid more than halfway out of the 40 mm travel range. The sliding mechanism contains 3D-printed tension springs to lock the moving magnet to one of the two positions.

Slider (Figure 11a-5, b-5) The slider tangible generates a numerical value from 0 mm (Figure 11b-5[1]) to 300 mm (Figure 11b-5[3]) based on the relative positions of two 5/8" magnets. The magnet at the base has its north pole positioned parallel to the slider, which also indicates the orientation of the tangible device. The second magnet slides on a laser-cut transparent acrylic sheet with markings engraved at every millimeter. The separation of the two magnets varies from 50 mm to 350 mm and is mapped to the 300 mm output range.
Knob - absolute (Figure 11a-6, b-6) The first design of the knob (absolute) contains a single 5/8" magnet positioned at the center of a rotatable upper part. The knob generates a numerical value from -180° to +180° based on the magnet's absolute horizontal orientation in MagDesk's coordinate frame, which is visually indicated by a 3D-printed arrowhead attached to the turning upper part. There are also markings at every 15 deg on the knob's lower part for visual reference.
Knob - relative (Figure 11a-7, b-7) The second design of the knob (relative) is modified from the first with an additional magnet affixed to the base of the knob, 56mm away from the turning magnet. The output value of the knob is determined by the relative angle between the two magnets. With this design, when the entire knob is rotated or moved on MagDesk, the output angle will remain the same, as the relative orientations of the magnets do not change.
Hinge (Figure 11a-8, b-8) The hinge tangible is similar to the knob (relative) but with the two magnets placed on the two branches of the hinge. Cutouts at the end of each arm allow the user to use the hinge as a protractor for measuring angles. The relative distance between the two magnets ranges from 100 mm when the hinge is fully closed (0°) to 164 mm when the hinge is fully opened (±180°).

5.2 Accuracy Evaluation

5.2.1 Evaluation Procedures. The accuracy and usability of the eight tangible primitives were evaluated individually. The evaluations of the (1) stylus and (6) knob (absolute) are omitted as they are functionally identical to individual magnets, whose positional and orientational accuracy have been analyzed comprehensively in Section 4.3.2. For the remaining tangible primitives, those with binary outputs, i.e., (2) button (momentary), (3) button (toggle), and (4) switch, were toggled 40 times on MagDesk's surface at each of the five testing locations shown in Figure 5a.

The tangibles that output numerical values, i.e., (5) slider, (7) knob (relative), and (8) hinge, were evaluated at the center of the table. The slider was adjusted manually using the engraved markings on the tangible as references, and measurements were taken for 5 seconds at every 10 mm. Similarly, the knob (relative) was adjusted using only the 3D-printed markings around the circumference of its base, with measurements taken for 10 seconds at every 15 deg. The hinge was evaluated in the same way as the knob, but its two arms were visually aligned to grids on a printed polar graph paper. Note that for all evaluations, MagDesk maintained *continuous 5-DoF tracking* for the magnets in the tangibles in addition to generating their output values.

5.2.2 Evaluation Results. The three tangible primitives with binary outputs, i.e., button (momentary), button (toggle), and switch, achieve 100% accuracy out of 200 samples. The measurements collected for the slider, knob (relative), and hinge are visualized in Figure 12 against the ground truth values. The average distance error for the slider is *1.03 mm* (SD: *0.63 mm*, N = 4950). The average angle error is *4.10 deg* (SD: *2.86 deg*, N = 7341) for the knob (relative) and *0.65 deg* (SD: *0.39 deg*, N = 7245) for the hinge. Since the relative differences in distance and angle between two magnets are used to generate tangible outputs, the average errors for both the slider and hinge are lower than the absolute positional and orientational errors of tracking a single 5/8"-diameter magnet at 50 mm height, which are *2.21 mm* and *0.74 deg*, respectively, as shown in Figure 8. The average angle error for the knob is higher at *4.10 deg*, with a wider distribution of predicted measurements toward the ±180° limit (Figure 12b). Because of the close proximity of the two magnets in the knob tangible, it becomes more challenging for the two-magnet solver to distinguish them when their polarity aligns. Note that for all evaluations conducted in

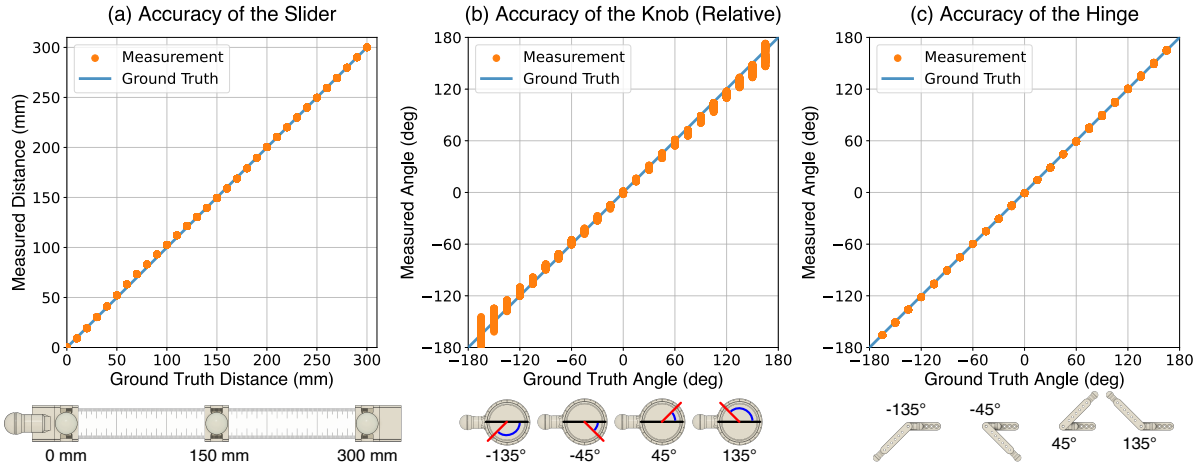

Fig. 12. Measurement accuracy of the (a) slider, (b) knob (relative), and (c) hinge tangibles, all of which involve two-magnet tracking.

this section, the tangibles were manipulated in an open loop with only physical markings on them as references to distance and angle. In an application that incorporates the tangibles primitives as controllers, the user could potentially achieve higher accuracy if they have access to real-time measurement readings as feedback, i.e., a closed-loop control.

5.3 Tangible Dashboard

To demonstrate the versatility and reconfigurability afforded by the tangible primitives, an interactive dashboard was implemented in Unity to visualize the poses and states of the tangibles.

5.3.1 Design and Implementation. Figure 13a shows the software schematic of initializing and tracking multiple tangible primitives. Seven initialization zones are defined on the MagDesk surface (Figure 13b). The two buttons (momentary / toggle) share the same location, as they are functionally identical for tracking purposes. When a user brings a tangible close to its corresponding initialization point (e.g., within 15 cm) that is not occupied by another object, the algorithm detects a new local maximum exceeding a threshold value in the magnitude of sensor readings, registers one of the seven types of tangibles, and creates a new instance of the analytical solver using that location as the seed point. Then, the software maintains continuous tracking of the newly added tangibles using the range of magnetometers specified in Table 3. Note that for tangibles with two spherical magnets, the two-magnet analytical solver will always be applied, and their positions and orientations are determined by interpolating the coordinates of the two embedded magnets. In addition, the software automatically groups two single-magnet tangibles with the same magnet size that are close to each other, e.g., two styluses or buttons, and applies the two-magnet solver.

To visualize the poses and states of the tangibles, the software pipeline sends the coordinates of the tangibles to a Unity program, as shown in Figure 13d. The Unity interface contains a complete 3D virtual representation of the table and all the tangibles on it. A projector mounted above MagDesk displays each tangible's output state beside it, i.e., binary or numerical values, while a separate monitor visualizes the entire setup (Figure 13c). As the user manipulates a tangible, the displayed value moves along it and updates in real-time.

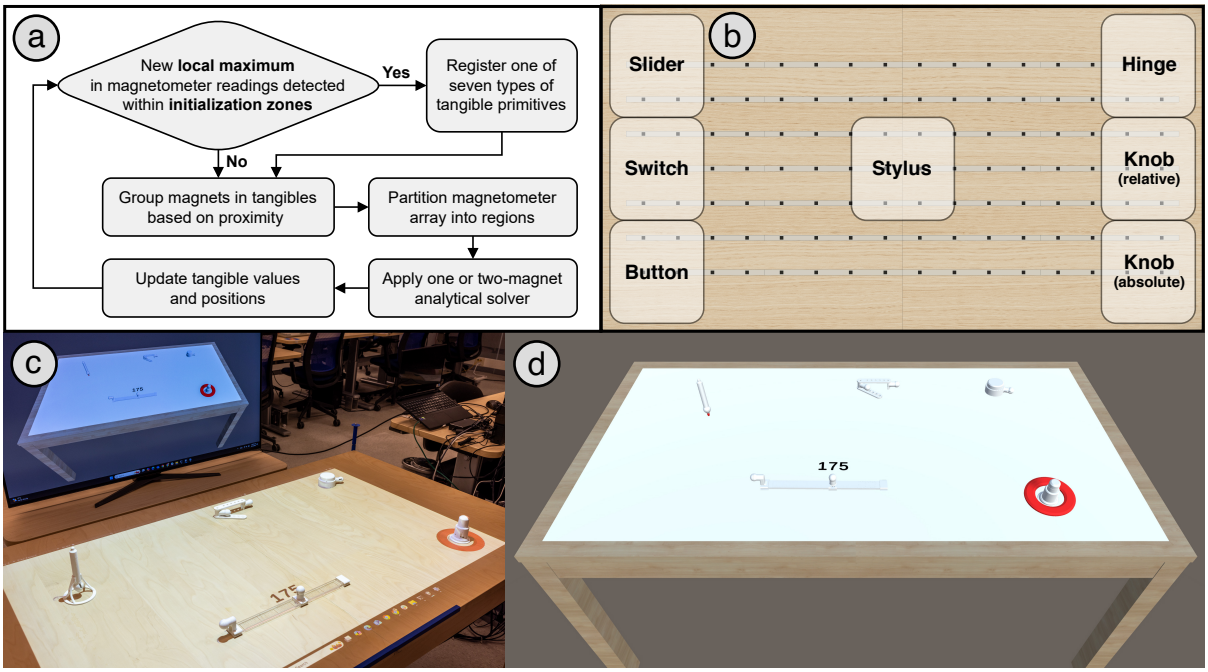

Fig. 13. A reconfigurable dashboard interface implemented using the tangible primitives. (a) The software schematic of initializing and tracking the tangible objects; (b) Seven locations defined on the MagDesk surface as the initialization zones; (c) Photo of several tangible primitives placed on MagDesk, with the output value projected beside the slider tangible; (d) Unity interface showing the same set of tangibles being tracked and visualized simultaneously in real-time.

5.3.2 *Discussions and Limitations of the Tangible Dashboard.*

Minimum Spacing between Tangibles. While MagDesk is able to robustly localize five tangibles with eight spherical magnets in real-time, as shown in Figure 13d, the minimum distance between adjacent tangibles presents a limitation on the maximum number of objects that could be tracked simultaneously. The two-magnet analytical solver introduced in Section 4.3.3 only accepts two magnets with the same dipole moment as input parameters. Therefore, in the current dashboard interface, two single-magnet solvers will be applied to two tangibles with different magnet sizes, e.g., a stylus and a button, even if they are in close proximity. In addition, MagDesk does not have separate solvers for more than two magnets. As a result, if three or more magnets are closer than the *Horizontal Radius* defined in Table 3, e.g., 300 mm for 5/8" magnets, their magnetic fields will have visible effects on each other, and the tracking accuracy will decrease. For future works, analytical solvers for more than two magnets (n-magnet solvers) that accept multiple different dipole moments as inputs could be implemented to offer more flexible positioning for multi-magnet tracking.

Predefined Initialization Zones. Since the analytical solver cannot distinguish between different types of tangibles or magnets of various strengths by itself, the dashboard interface specifies multiple initialization zones to which the user has to bring the tangibles close. Future works could reduce the user's burden by implementing a machine-learning model that automatically classifies the types of tangibles or sizes of magnets based on their magnetic signatures as they are added to the table.

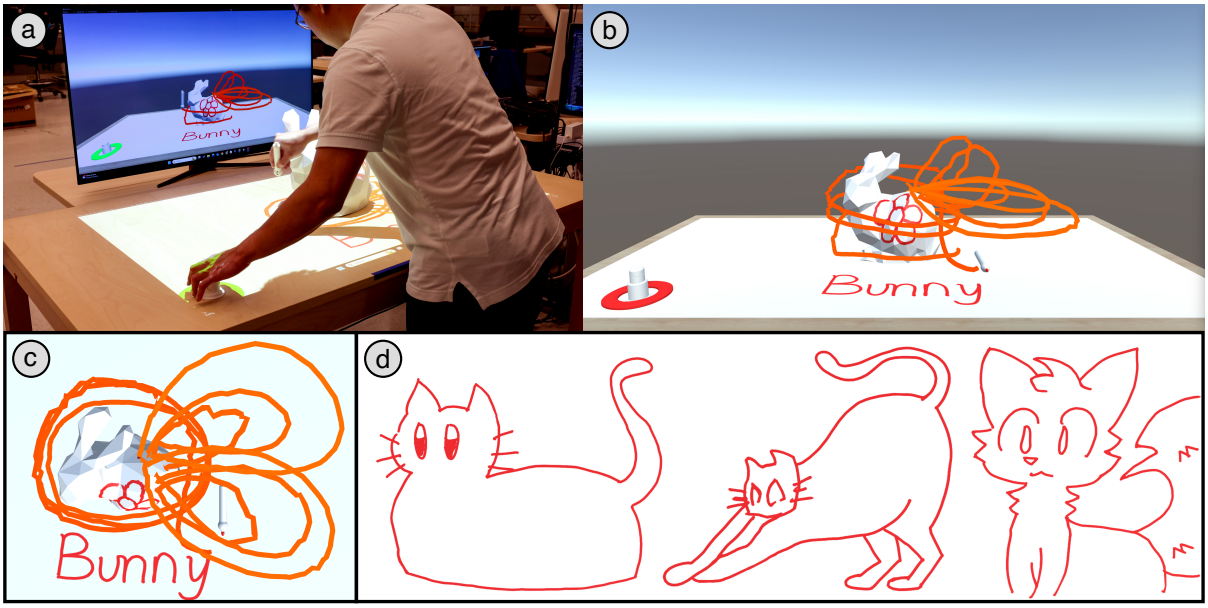

Fig. 14. 3D drawing interface controlled by magnetic tangibles. (a) The setup with a stylus for drawing 3D traces and a button tangible for controlling the activation of digital ink; (b) Traces drawn by the magnetic stylus both on 3D surfaces and in the air; (c) Top-down view showing a pair of wings attached to the bunny 3D model; (d) 2D sketches created by users on MagDesk surface.

6 Applications of MagDesk

The previous sections discussed the technical capabilities of MagDesk, highlighting its ability to track both a single magnet and multiple magnets simultaneously, along with specially designed tangible primitives. To assess if these capabilities are conducive to interactive user interfaces, several demo applications were developed and subjected to user testing. These applications include interactive 2D and 3D drawing tools, as well as various interactive games on a projection surface that utilize the tangible primitives.

6.1 3D Painting

MagDesk's accurate real-time tracking and large sensing volume present opportunities for 3D creativity by replacing traditional VR trackers and controllers [22] with magnetic tangibles. MagDesk's potential for 3D artistic creation was demonstrated through a 3D painting application implemented in Unity and controlled by tangible primitives introduced in Section 5.1. Figure 14a shows the physical setup, including a stylus for drawing 3D traces and a button for activating the digital ink, while Figure 14b-c visualize traces drawn by the magnetic stylus both on arbitrary 3D surfaces and in the air. In addition, Figure 14d shows example sketches created by users with the drawing application, demonstrating MagDesk's potential for artistic creation.

6.1.1 User Evaluation. Due to the challenges associated with quantitatively measuring MagDesk's accuracy at capturing user intentions, the first set of evaluations has been simplified to tracing the outlines of predetermined shapes using the magnetic stylus (Figure 11a-1). Then, assuming that the participants faithfully attempted to follow the predetermined shapes, we compared the output drawing of MagDesk to the predefined ground truth image. Another challenge is that creating three-dimensional paths for participants to trace easily is non-trivial. Therefore,

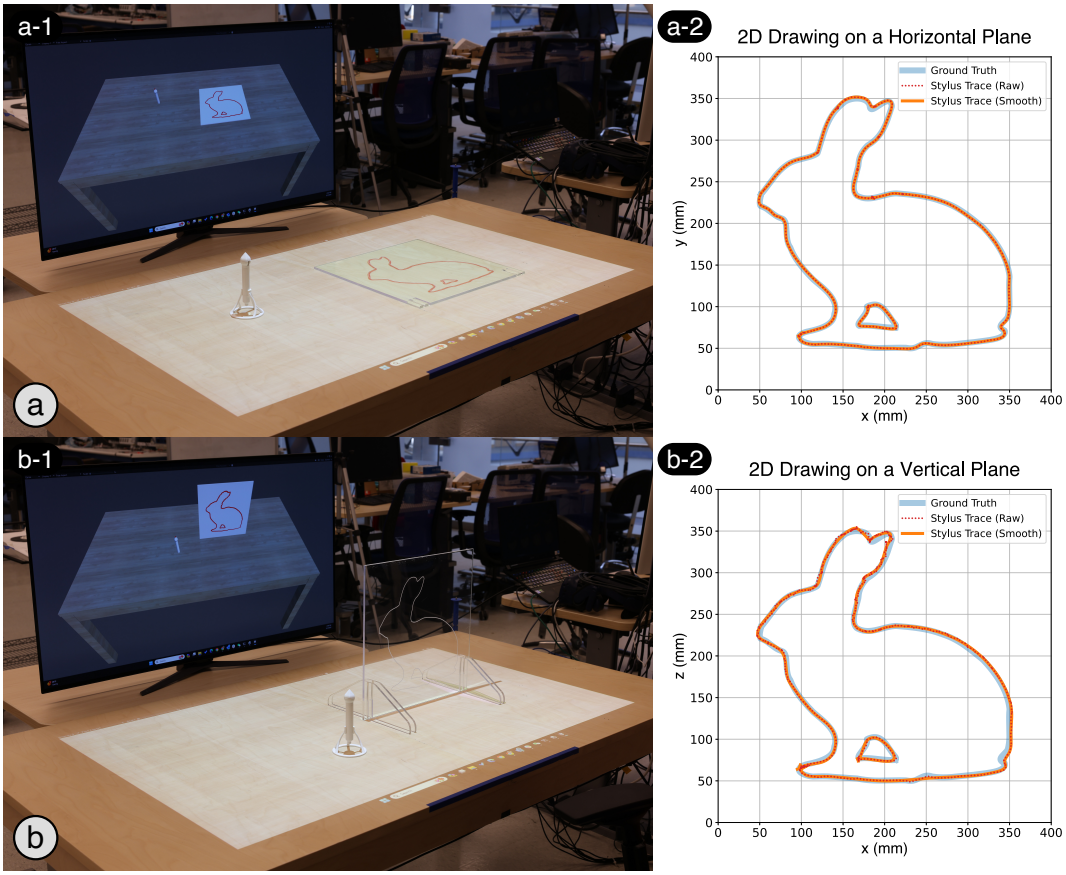

Fig. 15. User evaluation where the users traced the outline of a bunny in (a) horizontal and (b) vertical orientations. (a-1) and (b-1) show the physical setup for the evaluation. (a-2) and (b-2) show the raw and smoothed MagDesk stylus traces drawn by a user alongside the ground truth,

this evaluation was broken up into several sub-tasks, where participants were asked to draw in orthogonal planes covering MagDesk's tracking volume, i.e., one directly on MagDesk's table surface and the other set up vertically. While this method allows for easy quantitative measurement of the system's drawing accuracy, later subsections gave participants the opportunity to draw freehand in 3D without prompts or restrictions, after which qualitative feedback was solicited to understand their perceptions of the drawing capabilities of MagDesk.

Evaluation Setup. For the quantitative evaluation, a vector image of a bunny was lightly engraved onto a 40 cm × 40 cm acrylic sheet as a visual reference for the user. The pattern measures 30 cm × 30 cm and is centered on the sheet, as visualized by the light blue traces in Figure 15a-2 and b-2. The setup for the tangible dashboard was adapted for the user evaluation, and the user traced the outlines in both horizontal (Figure 15a-1) and vertical (Figure 15b-1) orientations. The stylus traces were projected directly onto MagDesk in real-time while the drawing board was flat on the table surface, and were displayed on the monitor while the board was positioned vertically. In the vertical orientation, the bunny pattern covers z-heights from 50 mm to 350 mm above the table surface. Eight users participated in the study.

Analysis and Results. To calculate the average error between the ground truth and stylus traces, the 3D coordinates of the stylus tip were projected onto the x-y plane for the horizontal orientation and the x-z plane for the vertical orientation. Then, the directed 2D Hausdorff distance between the stylus tip and ground truth, i.e., the shortest distance from the MagDesk-predicted coordinate to any part of the bunny pattern, was computed at each frame and averaged. On average, each stylus trace contains around 3200 data points, corresponding to 100 seconds of drawing duration.

Across all eight users, the average error is *0.73 mm* (SD: *0.61 mm*) for horizontal and *1.38 mm* (SD: *1.26 mm*) for vertical, as visualized in the red dotted traces in Figure 15a-2 and b-2. Note that both values are lower than the absolute positional error of tracking a single 3/4 in.-diameter magnet at 50 mm height, which is *2.49 mm*. This increased accuracy could be attributed to the fact that the tracking error in the axis perpendicular to the drawing plane is discarded to form a 2D projection. In addition, since coordinates in a drawing scenario form continuous traces instead of discrete points, noise reduction techniques such as cubic spline smoothing could be applied to improve the results, as visualized by the orange curves in Figure 15a-2 and b-2, which are common vectorization approaches used by many existing drawing applications.

6.1.2 Discussion. The previous section covered the quantitative measurement of 3D drawing accuracy. This section qualitatively assesses whether users found MagDesk effective as a drawing tool. After completing the tracing tasks, participants spent 3-5 minutes drawing freehand (one up to 10 minutes) and then rated the interface's intuitiveness, expressiveness, and effectiveness on a 1-7 Likert scale. At the study's conclusion, participants provided general feedback, which was transcribed and verified. The feedback was thematically analyzed to identify user perception trends.

Our study participants enjoyed sketching with the drawing interface and were able to express themselves artistically, with an example of user creation shown in Figure 14d. On average, the users rated 6.88 out of 7 (SD: 0.35) for its intuitiveness, 6.13 (SD: 0.84) for expressiveness, and 6.13 (SD: 0.84) for effectiveness. Out of the 19 comments we collected, three directly relate to the positive user experience. The users compared the interface to whiteboard drawing and commented that the stylus has a familiar form factor as a marker in terms of shape and weight (U2).

Eleven comments (58%) are related to additional features the users desire in the drawing application, including active sound feedback when the stylus touches the drawing surface to compensate for projector occlusion (U1, U3, U4), customizable trace color and thickness (U6, U8), and stylus textures that are sensitive to and adjusted based on the applied pressure or movement speed, i.e., thicker traces with higher pressure and thinner traces with higher velocity (U2, U5, U7). These suggestions are out of scope in the context of magnetic tracking and reflect areas for future enhancements to build a full-fledged drawing application. We interpreted them as evidence that MagDesk supports effective 3D drawing, and users prefer more functionalities to suit their personal needs.

The open-ended questions revealed two main drawbacks in the tracking capabilities of MagDesk, as identified from 19 comments. Firstly, users noted a latency issue in the drawing pipeline during fast stylus movements, with a noticeable delay between the stylus movement and the projected visualization (U3, U8). This latency is primarily caused by the data transfer and visualization of the magnet coordinates rather than the tracking pipeline itself. As discussed in Section 3.3.1, the combined data acquisition and solver prediction time stays within the 32.1 Hz update cycle. On average, collecting sensor readings from the 112 magnetometers requires 14.68 ms, and predicting the magnet coordinates using the analytical solver with its Python wrapper requires 7.61 ms. Therefore, the observed delay does not reflect the inherent limitation of MagDesk and could be further minimized through software engineering efforts.

Secondly, one user (U6) pointed out an issue with the refresh rate, stating that they could not sketch quickly due to the refresh rate causing smooth curves to appear as individual line segments. MagDesk's current implementation uses a 32.1 Hz sampling rate to optimize for lower measurement noise and higher tracking accuracy. However,

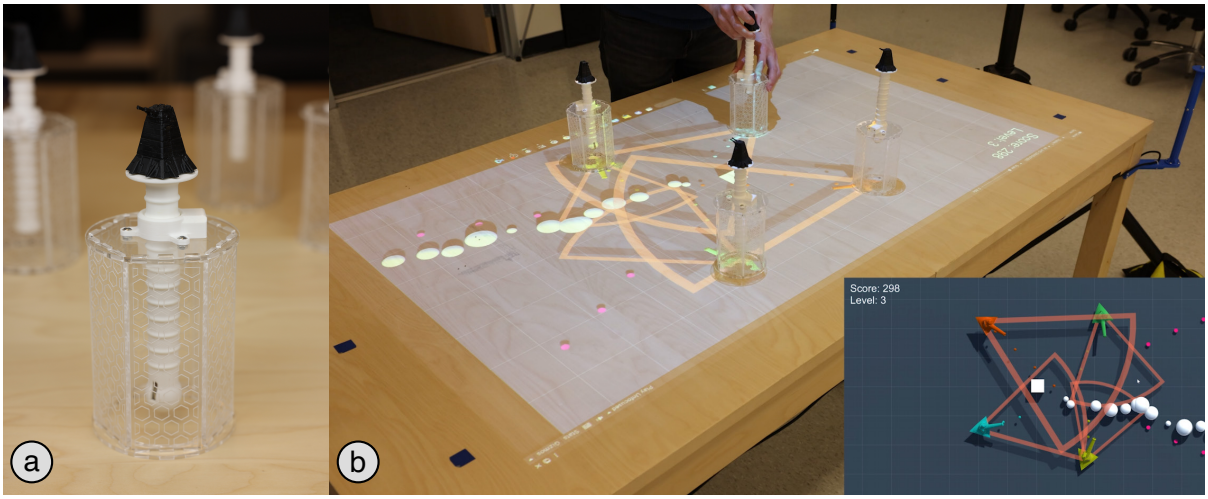

Fig. 16. A Tower Defense game implemented with MagDesk. (a) A tower game object with a 5/8" spherical magnet embedded near the bottom. (b) The gameplay showing four towers placed on MagDesk and the projected game interface (inset: screenshot of the game interface built in Unity).

the magnetometer (MLX90393) supports an update rate of up to 716.9 Hz with reduced noise performance. Future work could explore an adaptive refresh rate, employing a higher frequency near the table surface to support smoother user interactions and a lower frequency at height for more stable tracking.

6.1.3 Workshop Study for 3D Drawing. To further evaluate MagDesk's ability to facilitate 3D creativity with its large sensing volume, a workshop study was conducted with six participants to simulate a realistic tabletop workspace environment. The participants were introduced to the functionality of the magnetic stylus (Figure 11b-1) and an additional button (Figure 11b-3) for activating the digital ink so that the stylus could generate arbitrary 3D traces in midair. During the study, a large 3D-printed bunny with a *30 cm* height was positioned at the center of MagDesk, with its virtual representation being rendered on a monitor in front of the table (Figure 14a). In addition, an overhead projector would display any drawn trace onto the 3D-printed bunny as well as the table surface. During the study, the participants sat in front of MagDesk with their normal seating positions and were asked to (1) paint the back of the bunny with red ink and (2) cover both ears of the bunny with 3D traces in the air, e.g., creating a pair of earmuffs, by toggling the tangible button. At the end of the study, they were given opportunities to explore the interface freely and asked about their experience in terms of intuitiveness, usability, and comfort on a 1-7 Likert scale.

All six participants were able to complete the tasks successfully. On average, the users rated 6.67 out of 7 (SD: 0.47) for the interface's intuitiveness, 6 (SD: 0.58) for usability, and 6.5 (SD: 0.5) for comfort. The participants commented that the combination of the stylus and button tangibles supports intuitive controls and that the tracking range of MagDesk offers adequate space for 3D drawing.

6.2 Tangible Gaming

MagDesk offers opportunities for digital gaming by transforming game elements into trackable physical objects. MagDesk's potential for tangible gaming was demonstrated by a tower defense game implemented in Unity. Tower defense is a popular strategy game in which players defend their headquarters against attacking enemy waves by strategically placing defensive towers. Figure 16a shows the tower as a trackable game object with

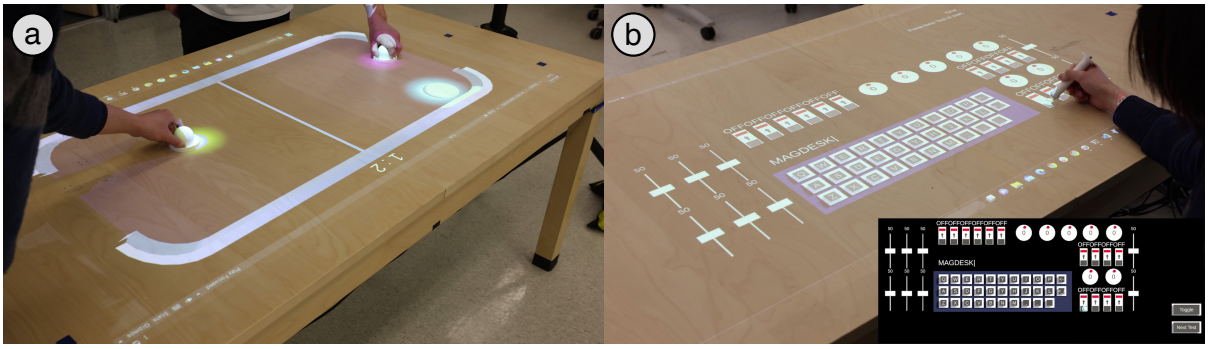

Fig. 17. A multi-player air hockey game (a) and a dashboard interface (b) implemented with MagDesk.

a 5/8 in. spherical magnet embedded in a custom-built structure. The magnet, with its north pole orientated horizontally, is attached to the bottom of a central column that can rotate and lock into various heights, combining a knob and slider from the tangible primitives (Figure 11b-5, b-6). The game interface was implemented in Unity and displayed on the table surface by a projector mounted directly above MagDesk. The interface was scaled such that its in-game unit corresponds to the physical dimension of MagDesk.

When the game initializes, four towers are placed at the four corners of MagDesk. Using these predefined coordinates as the seed positions, MagDesk acquires the 5-DoF poses of the four magnets and tracks them continuously using the approach described in Section 4.3.3. During the gameplay (Figure 16b), the enemies, represented as white spheres with larger ones containing more hit points (HP), emerge from the edge of the screen and move toward the player's base, represented as the white cube in the center. To defend the base and attack the enemy, the player has three options offered through manipulating the physical towers, i.e., changing the magnets' position and orientation:

- Moving a tower across the table surface changes its in-game coordinates.
- Rotating the central column changes the attack angle of the tower, represented by the orientation of the projected orange circular sector.
- Varying the height of the tower by pulling on the central column changes its attack range, represented by the size of the circular sector.

When an enemy enters the sector region of a tower, the tower automatically locks onto and shoots projectiles toward the enemy until its HP reaches zero and is eliminated. In addition, a higher tower with a longer attach range is programmed to have a lower rate of fire. This game mechanism encourages the player to strategically place the towers and balance between their attach range and damage output. The player scores points when an enemy is eliminated and loses points when it reaches the base. For every 100-point score increment, the game advances to the next level with more challenging enemies and an increased spawn rate.

Additionally, two more interactive interfaces are explored. Figure 17a depicts a classic air hockey game, where magnets are embedded in the physical paddles, and an overhead projector displays the air hockey puck, boundary walls, and game elements such as the scoreboard. Here, the MagDesk system measures the magnetic field induced by the magnet in the paddles using the array of magnetometers and calculates the locations of the two user paddles. This data is sent over TCP/IP to the Unity game engine, which calculates gameplay and renders the image of the puck. Figure 17b depicts an interactive dashboard memory game with the projector, and elements are manipulated using the tangible stylus. All three of these interfaces were demonstrated at a university Class Exposition where users were able to play the tangible games and compete against each other effectively.

7 Conclusion

MagDesk's ability to precisely and efficiently track passive magnets across expansive 3D spaces provides several improvements over traditional tracking technologies, especially within interactive tabletop environments. Utilizing a dense array of low-cost magnetometers paired with an advanced signal processing framework, MagDesk achieves exceptional accuracy in tracking and recognizing passive magnetic objects.

This system effectively overcomes common drawbacks associated with conventional tracking solutions, such as line-of-sight occlusion and the need for ongoing battery maintenance of powered transmitters. Furthermore, MagDesk significantly enhances the performance of magnetic tracking systems in terms of range and accuracy. The evaluations conducted underscore MagDesk's ability to reliably track multiple objects simultaneously in real time, positioning it as a superior alternative to previous methodologies. The practical implementations of MagDesk with several innovative tangible primitives and applications ranging from 3D drawing interfaces to augmented reality games, demonstrate its adaptability and capacity to enhance user interaction with engaging tangible interfaces. These attributes highlight MagDesk's potential to enrich both everyday and professional interactive environments.

Acknowledgments

The authors thank Sumukh Marathe for his early support on the physical construction of MagDesk and members of the Interactive Sensing and Computing Lab for their suggestions during paper revisions. We also appreciate the constructive feedback from our anonymous reviewers.

References

[1] [n. d.]. Intel RealSense. https://www.intelrealsense.com/compare-depth-cameras/. Accessed: April 25, 2024.
[2] 2024. Types of Motion Trackers. https://www.rokoko.com/insights/types-of-motion-trackers. Accessed: January 30, 2024.
[3] 2024. VIVE Tracker 3. https://www.vive.com/us/accessory/tracker3/. Accessed: January 30, 2024.
[4] Adafruit. 2017. Adafruit Feather nRF52 Bluefruit LE - nRF52832. https://www.adafruit.com/product/3406. Accessed: 2023-10-03.
[5] Sameer Agarwal, Keir Mierle, and The Ceres Solver Team. 2022. *Ceres Solver*. https://github.com/ceres-solver/ceres-solver
[6] Ananta Narayanan Balaji, Clayton Kimber, David Li, Shengzhi Wu, Ruofei Du, and David Kim. 2023. RetroSphere: Self-Contained Passive 3D Controller Tracking for Augmented Reality. *Proc. ACM Interact. Mob. Wearable Ubiquitous Technol.* 6, 4, Article 157 (jan 2023), 36 pages. https://doi.org/10.1145/3569479
[7] R.G. Brown and P.Y.C. Hwang. 1992. *Introduction to Random Signals and Applied Kalman Filtering*. Number v. 2 in Introduction to Random Signals and Applied Kalman Filtering. Wiley. https://books.google.com/books?id=6f5SAAAAMAAJ
[8] Yifeng Cao, Ashutosh Dhekne, and Mostafa Ammar. 2021. ITrackU: tracking a pen-like instrument via UWB-IMU fusion. In *Proceedings of the 19th Annual International Conference on Mobile Systems, Applications, and Services* (Virtual Event, Wisconsin) *(MobiSys '21)*. Association for Computing Machinery, New York, NY, USA, 453–466. https://doi.org/10.1145/3458864.3467885
[9] Dongyao Chen, Kang G. Shin, Yurong Jiang, and Kyu-Han Kim. 2017. Locating and Tracking BLE Beacons with Smartphones. In *Proceedings of the 13th International Conference on Emerging Networking EXperiments and Technologies* (Incheon, Republic of Korea) *(CoNEXT '17)*. Association for Computing Machinery, New York, NY, USA, 263–275. https://doi.org/10.1145/3143361.3143385
[10] Dongyao Chen, Mingke Wang, Chenxi He, Qing Luo, Yasha Iravantchi, Alanson Sample, Kang G. Shin, and Xinbing Wang. 2021. MagX: Wearable, Untethered Hands Tracking with Passive Magnets *(MobiCom '21)*. Association for Computing Machinery, New York, NY, USA, 269–282. https://doi.org/10.1145/3447993.3483260
[11] Ke-Yu Chen, Shwetak N. Patel, and Sean Keller. 2016. Finexus: Tracking Precise Motions of Multiple Fingertips Using Magnetic Sensing. In *Proceedings of the 2016 CHI Conference on Human Factors in Computing Systems* (San Jose, California, USA) *(CHI '16)*. Association for Computing Machinery, New York, NY, USA, 1504–1514. https://doi.org/10.1145/2858036.2858125
[12] Mingshi Chen, Panlong Yang, Jie Xiong, Maotian Zhang, Youngki Lee, Chaocan Xiang, and Chang Tian. 2019. Your Table Can Be an Input Panel: Acoustic-based Device-Free Interaction Recognition. *Proc. ACM Interact. Mob. Wearable Ubiquitous Technol.* 3, 1, Article 3 (mar 2019), 21 pages. https://doi.org/10.1145/3314390
[13] Michael Chesser, Leon Chea, and Damith C. Ranasinghe. 2018. Field Deployable Real-Time Indoor Spatial Tracking System for Human Behavior Observations. In *Proceedings of the 16th ACM Conference on Embedded Networked Sensor Systems* (Shenzhen, China) *(SenSys '18)*. Association for Computing Machinery, New York, NY, USA, 369–370. https://doi.org/10.1145/3274783.3275187

[14] Krishna Chintalapudi, Anand Padmanabha Iyer, and Venkata N. Padmanabhan. 2010. Indoor localization without the pain. In *Proceedings of the Sixteenth Annual International Conference on Mobile Computing and Networking* (Chicago, Illinois, USA) *(MobiCom '10)*. Association for Computing Machinery, New York, NY, USA, 173–184. https://doi.org/10.1145/1859995.1860016

[15] T.L. Chow. 2006. *Introduction to Electromagnetic Theory: A Modern Perspective*. Jones and Bartlett Publishers. https://books.google.com/books?id=dpnpMhw1zo8C

[16] A.I. Comport, E. Marchand, M. Pressigout, and F. Chaumette. 2006. Real-time markerless tracking for augmented reality: the virtual visual servoing framework. *IEEE Transactions on Visualization and Computer Graphics* 12, 4 (2006), 615–628. https://doi.org/10.1109/TVCG.2006.78

[17] HTC Corporation. 2021. Introducing VIVE Tracker (3.0). https://www.vive.com/us/accessory/tracker3/. Accessed: 2023-10-03.

[18] B.D. Cullity and C.D. Graham. 2009. *Introduction to Magnetic Materials*. Wiley. https://ieeexplore.ieee.org/book/5361017

[19] Meenu Rani Dey, Satadal Sengupta, Bhabendu Kr. Mohanta, Debasish Jena, and Sandip Chakraborty. 2018. Magneto: Leveraging Magnetic Field Changes for Inferring Smartphone App Usage. In *Proceedings of the 24th Annual International Conference on Mobile Computing and Networking* (New Delhi, India) *(MobiCom '18)*. Association for Computing Machinery, New York, NY, USA, 777–779. https://doi.org/10.1145/3241539.3267772

[20] Chuhan Gao, Xinyu Zhang, and Suman Banerjee. 2018. Conductive Inkjet Printed Passive 2D TrackPad for VR Interaction. In *Proceedings of the 24th Annual International Conference on Mobile Computing and Networking* (New Delhi, India) *(MobiCom '18)*. Association for Computing Machinery, New York, NY, USA, 83–98. https://doi.org/10.1145/3241539.3241546

[21] Jun Gong, Aakar Gupta, and Hrvoje Benko. 2020. Acustico: Surface Tap Detection and Localization using Wrist-based Acoustic TDOA Sensing. In *Proceedings of the 33rd Annual ACM Symposium on User Interface Software and Technology* (Virtual Event, USA) *(UIST '20)*. Association for Computing Machinery, New York, NY, USA, 406–419. https://doi.org/10.1145/3379337.3415901

[22] Google. 2016. Tilt Brush by Google. https://www.tiltbrush.com/. Accessed: 2024-04-10.

[23] Hua Huang, Hongkai Chen, and Shan Lin. 2019. MagTrack: Enabling Safe Driving Monitoring with Wearable Magnetics. In *Proceedings of the 17th Annual International Conference on Mobile Systems, Applications, and Services* (Seoul, Republic of Korea) *(MobiSys '19)*. Association for Computing Machinery, New York, NY, USA, 326–339. https://doi.org/10.1145/3307334.3326107

[24] Yasha Iravantchi, Yi Zhao, Kenrick Kin, and Alanson P. Sample. 2023. SAWSense: Using Surface Acoustic Waves for Surface-bound Event Recognition. In *Proceedings of the 2023 CHI Conference on Human Factors in Computing Systems* (Hamburg, Germany) *(CHI '23)*. Association for Computing Machinery, New York, NY, USA, Article 422, 18 pages. https://doi.org/10.1145/3544548.3580991

[25] J.D. Jackson. 2012. *Classical Electrodynamics*. Wiley. https://books.google.com/books?id=8qHCZjJHRUgC

[26] Wenzel Jakob, Jason Rhinelander, and Dean Moldovan. 2017. pybind11 – Seamless operability between C++11 and Python. https://github.com/pybind/pybind11.

[27] Han-Chih Kuo, Rong-Hao Liang, Long-Fei Lin, and Bing-Yu Chen. 2016. GaussMarbles: Spherical Magnetic Tangibles for Interacting with Portable Physical Constraints. In *Proceedings of the 2016 CHI Conference on Human Factors in Computing Systems* (San Jose, California, USA) *(CHI '16)*. Association for Computing Machinery, New York, NY, USA, 4228–4232. https://doi.org/10.1145/2858036.2858559

[28] Jiachen Li, Bin Wang, Shiqiang Zhu, Xin Cao, Fan Zhong, Wenxuan Chen, Te Li, Jason Gu, and Xueying Qin. 2022. BCOT: A Markerless High-Precision 3D Object Tracking Benchmark. In *2022 IEEE/CVF Conference on Computer Vision and Pattern Recognition (CVPR)*. 6687–6696. https://doi.org/10.1109/CVPR52688.2022.00658

[29] Rong-Hao Liang, Liwei Chan, Hung-Yu Tseng, Han-Chih Kuo, Da-Yuan Huang, De-Nian Yang, and Bing-Yu Chen. 2014. GaussBricks: magnetic building blocks for constructive tangible interactions on portable displays. In *Proceedings of the SIGCHI Conference on Human Factors in Computing Systems* (Toronto, Ontario, Canada) *(CHI '14)*. Association for Computing Machinery, New York, NY, USA, 3153–3162. https://doi.org/10.1145/2556288.2557105

[30] Rong-Hao Liang, Kai-Yin Cheng, Liwei Chan, Chuan-Xhyuan Peng, Mike Y. Chen, Rung-Huei Liang, De-Nian Yang, and Bing-Yu Chen. 2013. GaussBits: magnetic tangible bits for portable and occlusion-free near-surface interactions. In *Proceedings of the SIGCHI Conference on Human Factors in Computing Systems* (Paris, France) *(CHI '13)*. Association for Computing Machinery, New York, NY, USA, 1391–1400. https://doi.org/10.1145/2470654.2466185

[31] Rong-Hao Liang, Kai-Yin Cheng, Chao-Huai Su, Chien-Ting Weng, Bing-Yu Chen, and De-Nian Yang. 2012. GaussSense: attachable stylus sensing using magnetic sensor grid. In *Proceedings of the 25th Annual ACM Symposium on User Interface Software and Technology* (Cambridge, Massachusetts, USA) *(UIST '12)*. Association for Computing Machinery, New York, NY, USA, 319–326. https://doi.org/10.1145/2380116.2380157

[32] Rong-Hao Liang, Han-Chih Kuo, Liwei Chan, De-Nian Yang, and Bing-Yu Chen. 2014. GaussStones: shielded magnetic tangibles for multi-token interactions on portable displays. In *Proceedings of the 27th Annual ACM Symposium on User Interface Software and Technology* (Honolulu, Hawaii, USA) *(UIST '14)*. Association for Computing Machinery, New York, NY, USA, 365–372. https://doi.org/10.1145/2642918.2647384

[33] Manni Liu, Linsong Cheng, Kun Qian, Jiliang Wang, Jin Wang, and Yunhao Liu. 2020. Indoor acoustic localization: A survey. *Human-centric Computing and Information Sciences* 10 (2020), 1–24.

[34] Yihao Liu, Kai Huang, Xingzhe Song, Boyuan Yang, and Wei Gao. 2020. MagHacker: eavesdropping on stylus pen writing via magnetic sensing from commodity mobile devices. In *Proceedings of the 18th International Conference on Mobile Systems, Applications, and Services* (Toronto, Ontario, Canada) *(MobiSys '20)*. Association for Computing Machinery, New York, NY, USA, 148–160. https://doi.org/10.1145/3386901.3389030

[35] Yunfei Ma, Nicholas Selby, and Fadel Adib. 2017. Minding the Billions: Ultra-wideband Localization for Deployed RFID Tags. In *Proceedings of the 23rd Annual International Conference on Mobile Computing and Networking* (Snowbird, Utah, USA) *(MobiCom '17)*. Association for Computing Machinery, New York, NY, USA, 248–260. https://doi.org/10.1145/3117811.3117833

[36] K&J Magnetics. 2024. N42 Sphere Magnets. https://www.kjmagnetics.com/products.asp?cat=12/. Accessed: 2024-05-01.

[37] Ben Maman and Amit Bermano. 2022. TypeNet: Towards Camera Enabled Touch Typing on Flat Surfaces through Self-Refinement. In *2022 IEEE/CVF Winter Conference on Applications of Computer Vision (WACV)*. 567–576. https://doi.org/10.1109/WACV51458.2022.00064

[38] Melexis. 2023. MLX90393: Triaxis Magnetic Node Datasheet. https://www.melexis.com/en/documents/documentation/datasheets/datasheet-mlx90393.pdf. Accessed: 2023-10-03.

[39] J J More. 1977. Levenberg–Marquardt algorithm: implementation and theory. (1 1977). https://www.osti.gov/biblio/7256021

[40] Farshid Salemi Parizi, Eric Whitmire, and Shwetak Patel. 2020. AuraRing: Precise Electromagnetic Finger Tracking. *Proc. ACM Interact. Mob. Wearable Ubiquitous Technol.* 3, 4, Article 150 (sep 2020), 28 pages. https://doi.org/10.1145/3369831

[41] Mark Richardson, Matt Durasoff, and Robert Wang. 2020. Decoding Surface Touch Typing from Hand-Tracking. In *Proceedings of the 33rd Annual ACM Symposium on User Interface Software and Technology* (Virtual Event, USA) *(UIST '20)*. Association for Computing Machinery, New York, NY, USA, 686–696. https://doi.org/10.1145/3379337.3415816

[42] Yang-Hsi Su, Chouchang Jack Yang, Euiseok Hwang, and Alanson P. Sample. 2023. Single Packet, Single Channel, Switched Antenna Array for RF Localization. 7, 2, Article 76 (jun 2023), 25 pages. https://doi.org/10.1145/3596263

[43] Hemant Bhaskar Surale, Aakar Gupta, Mark Hancock, and Daniel Vogel. 2019. TabletInVR: Exploring the Design Space for Using a Multi-Touch Tablet in Virtual Reality. In *Proceedings of the 2019 CHI Conference on Human Factors in Computing Systems* (Glasgow, Scotland Uk) *(CHI '19)*. Association for Computing Machinery, New York, NY, USA, 1–13. https://doi.org/10.1145/3290605.3300243

[44] Cameron R. Taylor, Haley G. Abramson, and Hugh M. Herr. 2019. Low-Latency Tracking of Multiple Permanent Magnets. *IEEE Sensors Journal* 19, 23 (2019), 11458–11468. https://doi.org/10.1109/JSEN.2019.2936766

[45] Lihao Wang, Wei Wang, Haipeng Dai, and Shizhe Liu. 2023. MagSound: Magnetic Field Assisted Wireless Earphone Tracking. *Proc. ACM Interact. Mob. Wearable Ubiquitous Technol.* 7, 1, Article 33 (mar 2023), 32 pages. https://doi.org/10.1145/3580889

[46] Mingke Wang, Qing Luo, Yasha Iravantchi, Xiaomeng Chen, Alanson Sample, Kang G. Shin, Xiaohua Tian, Xinbing Wang, and Dongyao Chen. 2022. Automatic calibration of magnetic tracking. In *Proceedings of the 28th Annual International Conference on Mobile Computing And Networking* (Sydney, NSW, Australia) *(MobiCom '22)*. Association for Computing Machinery, New York, NY, USA, 391–404. https://doi.org/10.1145/3495243.3558760

[47] Pierre Wellner. 1993. Interacting with Paper on the DigitalDesk. *Commun. ACM* 36, 7 (jul 1993), 87–96. https://doi.org/10.1145/159544.159630

[48] Eric Whitmire, Farshid Salemi Parizi, and Shwetak Patel. 2019. Aura: Inside-out Electromagnetic Controller Tracking. In *Proceedings of the 17th Annual International Conference on Mobile Systems, Applications, and Services* (Seoul, Republic of Korea) *(MobiSys '19)*. Association for Computing Machinery, New York, NY, USA, 300–312. https://doi.org/10.1145/3307334.3326090

[49] Po-Chen Wu, Robert Wang, Kenrick Kin, Christopher Twigg, Shangchen Han, Ming-Hsuan Yang, and Shao-Yi Chien. 2017. DodecaPen: Accurate 6DoF Tracking of a Passive Stylus. In *Proceedings of the 30th Annual ACM Symposium on User Interface Software and Technology* (Québec City, QC, Canada) *(UIST '17)*. Association for Computing Machinery, New York, NY, USA, 365–374. https://doi.org/10.1145/3126594.3126664

[50] Yang Zhang, Gierad Laput, and Chris Harrison. 2017. Electrick: Low-Cost Touch Sensing Using Electric Field Tomography. In *Proceedings of the 2017 CHI Conference on Human Factors in Computing Systems* (Denver, Colorado, USA) *(CHI '17)*. Association for Computing Machinery, New York, NY, USA, 1–14. https://doi.org/10.1145/3025453.3025842

[51] Qian Zhou, George Fitzmaurice, and Fraser Anderson. 2022. In-Depth Mouse: Integrating Desktop Mouse into Virtual Reality. In *Proceedings of the 2022 CHI Conference on Human Factors in Computing Systems* (New Orleans, LA, USA) *(CHI '22)*. Association for Computing Machinery, New York, NY, USA, Article 354, 17 pages. https://doi.org/10.1145/3491102.3501884

A Appendix

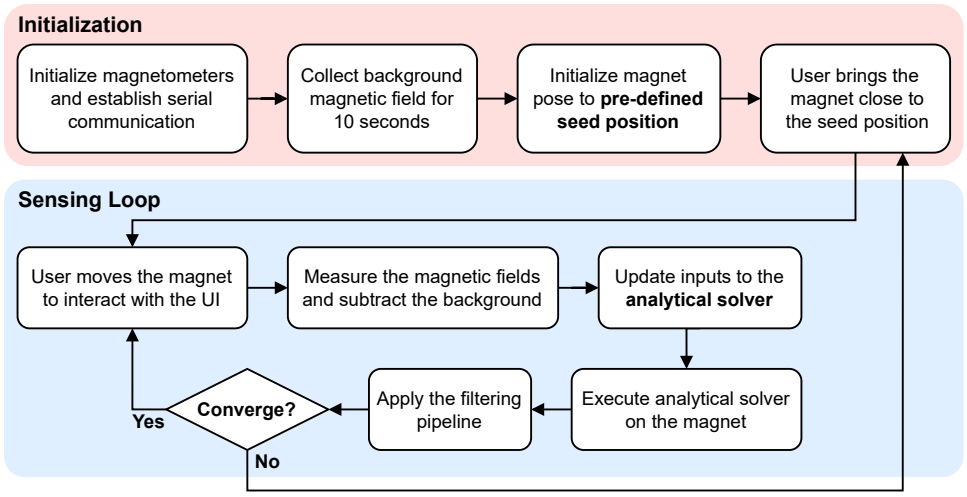

Fig. 18. MagDesk's software schematics, including the initialization phase and sensing loop.

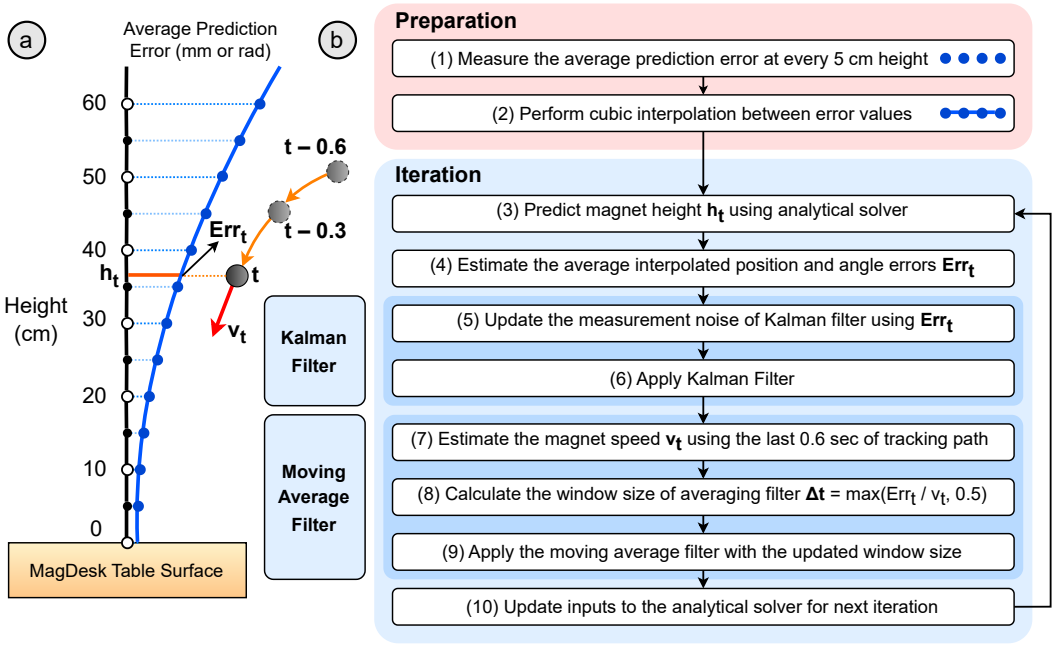

Fig. 19. Schematics of MagDesk's adaptive filtering pipeline which combines a Kalman filter and windowed moving average filter.

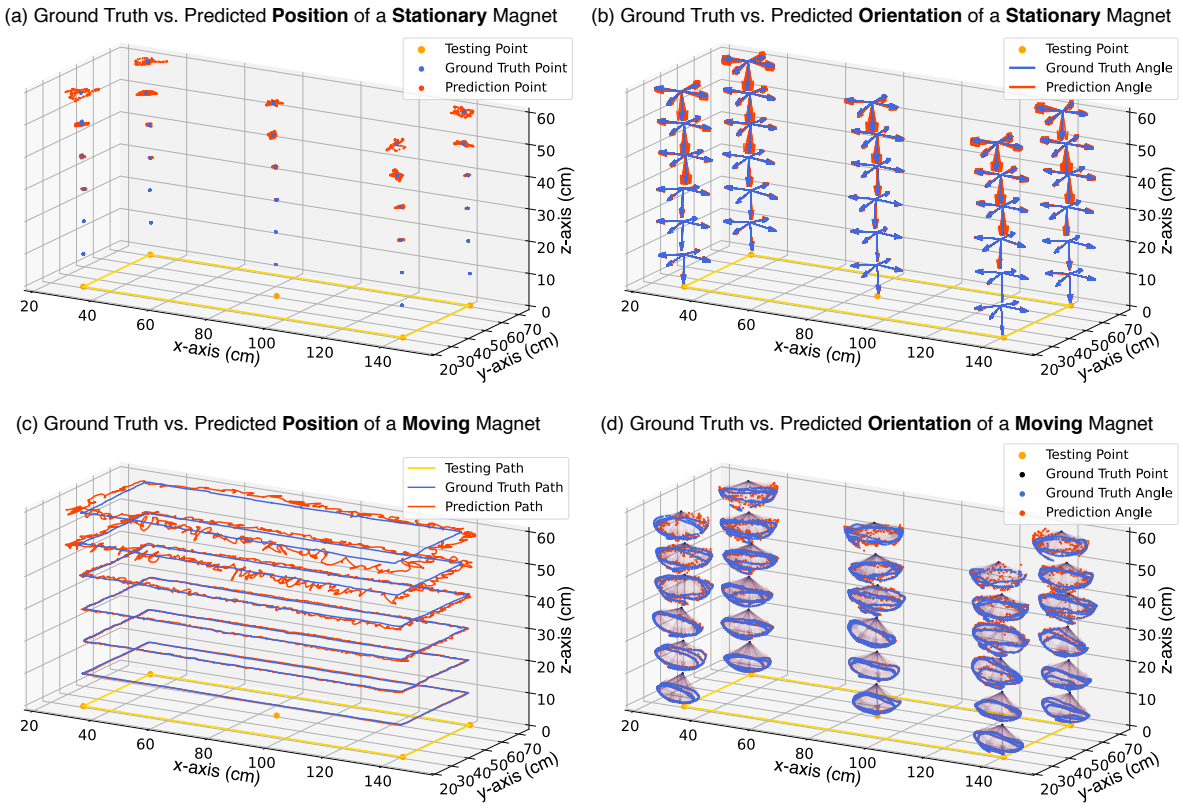

Fig. 20. Visualization of the ground truth and predicted position and orientation collected during the tracking experiments. The results are plotted for heights from 10 cm to 60 cm every 10 cm. For (c), the path for 20 mm/s movement speed is plotted. For (d), the dots in the scatter plot highlight the endpoints of vectors representing the ground truth and predicted orientation as the magnet was rotated around fixed locations. For all plots, the overlapping and alignments between the ground truth and prediction demonstrate high tracking accuracy.

Magnet Diameter	Magnet Weight	Dipole Moment
1/2" (12.7 mm)	8.05 g	1.13 A·m^2
5/8" (15.9 mm)	15.7 g	2.20 A·m^2
3/4" (19.0 mm)	**27.2 g**	**3.80 A·m^2**
1" (25.4 mm)	64.4 g	9.01 A·m^2

Table 6. List of magnet sizes evaluated for tracking performance.